

1 **An antisense RNA capable of modulating the
2 expression of the tumor suppressor microRNA-34a**
3

4 **Jason T. Serviss^{1*}, Felix Clemens Richter^{1,2}, Nathanael Johansson
5 Andrews¹, Miranda Houtman, Laura Schwarzmüller, Per Johnsson,
6 Jimmy Van Den Eynden, Erik Larsson³, Dan Grandér¹, Katja Pokrovskaia
7 Tamm¹**

8
9 ¹ Department of Oncology and Pathology, Karolinska Institutet, Stockholm,
10 Sweden

11 ² Kennedy Institute of Rheumatology, University of Oxford, Roosevelt Drive,
12 Oxford OX3 7FY, UK

13 ³Department of Medical Biochemistry and Cell Biology, Institute of
14 Biomedicine, The Sahlgrenska Academy, University of Gothenburg, SE-405
15 30 Gothenburg, Sweden

16 *** Correspondence:**

17 Jason T. Serviss, Department of Oncology and Pathology, Karolinska
18 Institutet, Stockholm, Sweden, SE-17177. jason.serviss@ki.se

21 **Abstract**

23 The microRNA-34a is a well-studied tumor suppressor microRNA (miRNA)
24 that is a direct down-stream target of TP53 and has roles in multiple pathways
25 associated with oncogenesis, such as proliferation, cellular growth, and
26 differentiation. Due to its wide variety of targets that suppress oncogenesis, it
27 is not surprising that miR34a expression has been shown to be dys-regulated
28 in a wide variety of both solid tumors and hematological malignancies.
29 Despite this, the mechanisms by which miR34a is regulated in these cancers
30 is not well studied. Here we find that the *miR34a* antisense RNA, a long non-
31 coding RNA transcribed antisense to *miR34a*, is critical
32 for *miR34a* expression and mediation of its cellular functions in multiple types
33 of human cancer. In addition, we characterize miR34a asRNA's ability to
34 facilitate miR34a expression under multiple types of cellular stress in both
35 TP53 deficient and wild-type settings.

36 **Introduction**

37 In recent years advances in functional genomics has revolutionized our
38 understanding of the human genome. Evidence now points to the fact that
39 approximately 75% of the genome is transcribed but only ~1.2% of this is
40 responsible for encoding proteins (International Human Genome Sequencing
41 2004, Djebali et al. 2012). Of these recently identified elements, long non-
42 coding (lnc) RNAs are defined as transcripts exceeding 200bp in length with a
43 lack of a functional open reading frame. Some lncRNAs are dually classified
44 as antisense (as) RNAs that are expressed from the same locus as a sense
45 transcript in the opposite orientation. Current estimates using high-throughput
46 transcriptome sequencing, indicate that up to 20-40% of the approximately
47 20,000 protein-coding genes exhibit antisense transcription (Chen et al. 2004,
48 Katayama et al. 2005, Ozsolak et al. 2010). The hypothesis that asRNAs play
49 an important role in oncogenesis was first proposed when studies increasingly
50 found examples of aberrant expression of these transcripts and other lncRNA
51 subgroups in tumor samples (Balbin et al. 2015). Although studies
52 characterizing the functional importance of asRNAs in cancer are limited to
53 date, characterization a number of individual transcripts has led to the
54 discovery of multiple examples of asRNA-mediated regulation of several well
55 known tumorigenic factors (Yap et al. 2010, Johnsson et al. 2013). The
56 mechanisms by which asRNAs accomplish this are diverse, and include
57 recruitment of chromatin modifying factors (Rinn et al. 2007), acting as
58 microRNA (miRNA) sponges (Memczak et al. 2013), and causing
59 transcriptional interference (Conley et al. 2012).

60

61 Responses to cellular stress, e.g. DNA damage, sustained oncogene
62 expression, and nutrient deprivation, are all tightly monitored and orchestrated
63 cellular pathways that are commonly dys-regulated in cancer. Cellular
64 signaling in response to these types of cellular stress often converge on the
65 transcription factor *TP53* that regulates transcription of coding and non-coding
66 downstream targets. One non-coding target of *TP53* is the tumor suppressor
67 microRNA known as *miR34a* (Raver-Shapira et al. 2007).
68 Upon *TP53* activation *miR34a* expression is increased allowing it to down-
69 regulate its targets involved in cellular pathways such as, growth factor
70 signaling, apoptosis, differentiation, and cellular senescence (Lal et al. 2011,
71 Slabakova et al. 2017). *miR34a* is a crucial factor in mediating activated *TP53*
72 response and it is often deleted or down-regulated in human cancers and has
73 also been shown to be a valuable prognostic marker (Cole et al. 2008,
74 Gallardo et al. 2009, Zenz et al. 2009, Cheng et al. 2010, Liu et al. 2011).
75 Reduced *miR34a* transcription is mediated via epigenetic regulation in many
76 solid tumors, such as colorectal-, pancreatic-, and ovarian cancer (Vogt et al.
77 2011), as well as multiple types of hematological malignancies (Chim et al.
78 2010). In addition, *miR34a* has been shown to be transcriptionally regulated
79 via *TP53* homologs, *TP63* and *TP73*, other transcription factors, e.g. *STAT3*
80 and *MYC*, and, in addition, post-transcriptionally through miRNA sponging by
81 the *NEAT1* lncRNA (Chang et al. 2008, Su et al. 2010, Agostini et al. 2011,
82 Rokavec et al. 2015, Ding et al. 2017). Despite these findings, the
83 mechanisms underlying *miR34a* regulation in the context of oncogenesis have
84 not yet been fully elucidated.

85

86 Studies across multiple cancer types have reported a decrease in oncogenic
87 phenotypes when miR34a expression is induced in a p53-null background,
88 although endogenous mechanisms for achieving this have not yet been
89 discovered (Liu et al. 2011, Ahn et al. 2012, Yang et al. 2012, Stahlhut et al.
90 2015, Wang et al. 2015). In addition, previous reports have identified a
91 lncRNA originating in the antisense orientation from the miR34a locus which
92 is regulated by TP53 and is induced upon cellular stress (Rashi-Elkeles et al.
93 2014, Hunten et al. 2015, Leveille et al. 2015, Ashouri et al. 2016, Kim et al.
94 2017). Despite this, none of these studies have continued to functionally
95 characterize this transcript. In this study we functionally characterize
96 the *miR34a* asRNA transcript, and find that modulating the levels of
97 the *miR34a* asRNA is sufficient to increase levels of *miR34a* and results in a
98 decrease of multiple tumorigenic phenotypes. Furthermore, we find that
99 miR34a asRNA-mediated up-regulation of miR34a is sufficient to induce
100 endogenous cellular mechanisms counteracting several types of stress stimuli
101 in a *TP53* deficient background. Finally, similar to the functional roles of
102 antisense transcription at protein-coding genes, we find that antisense RNAs
103 are also capable of regulating cancer-associated miRNAs.

104

105 **Results**

106

107 ***miR34a* asRNA is a broadly expressed, non-coding transcript whose**
108 **levels correlate with *miR34a* expression**

109

110 *miR34a* asRNA is transcribed in a “head-to-head” orientation with
111 approximately 100 base pair overlap with the *miR34a* host gene (HG) (**Fig.**
112 **1a**). Due to the fact that sense/antisense pairs can be both concordantly and
113 discordantly expressed, we sought to evaluate this relationship in the case of

114 *miR34a* HG and its asRNA. Using a diverse panel of cancer cell lines, we
115 detected co-expression of both the *miR34a* HG and *miR34a* asRNA (**Fig. 1b**).
116 We included *TP53*+/+, *TP53* mutated, and *TP53*-/- cell lines in the panel due
117 to previous reports that *miR34a* is a known downstream target of TP53.
118 These results indicate that *miR34a* HG and *miR34a* asRNA are co-expressed
119 and that their expression levels correlate with *TP53* status, with *TP53*-/- cell
120 lines tending to have decreased expression of both transcripts.

121

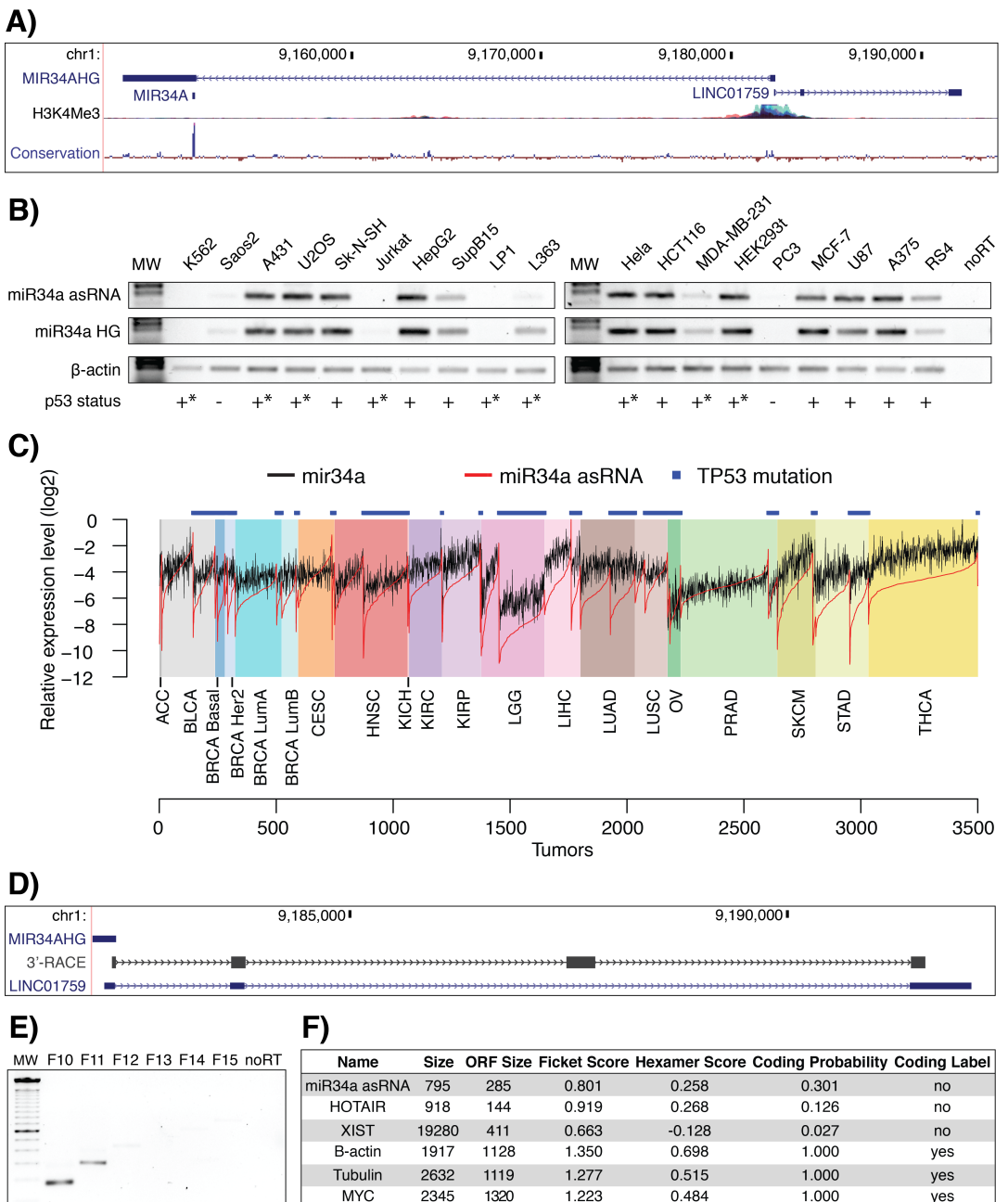


Figure 1: Characterization of the *miR34a* asRNA transcript. **A)** Architecture of the *miR34a* locus (hg38, RefSeq) including *miR34a* HG, mature *miR34a*, and miR34a asRNA (*LINC01759*). H3K4me3 ChIP-seq data, indicating the active promoter region, and conservation are also shown. **B)** Semi-quantitative PCR data from the screening of a panel of cancer cell lines. *Indicates either mutated *TP53* or wild-type *TP53* with mechanisms present, which inhibit *TP53* function (e.g. SV40 large T antigen in HEK293T cells). **C)** Graphical depiction of the TCGA correlation analysis. The *TP53* mutation samples only include nonsynonymous *TP53* mutations (corresponding statistics in Figure 1-Supplement 1). Adrenocortical carcinoma (ACC), Bladder Urothelial Carcinoma (BLCA), Breast invasive carcinoma (BRCA), Head and Neck squamous cell carcinoma (HNSC), Kidney Chromophobe (KICH), Lower Grade Glioma (LGG), Liver hepatocellular carcinoma (LIHC), Ovarian serous cystadenocarcinoma (OV), Prostate adenocarcinoma (PRAD), Skin Cutaneous Melanoma (SKCM), Stomach adenocarcinoma (STAD). **D)** 3'-RACE sequencing results and the annotated *miR34a* asRNA (*LINC01759*). **E)** Semi-quantitative PCR results from the primer walk assay (i.e. forward primers staggered upstream of the transcripts annotated start site) performed using HEK293T cells (Figure 1 Supplement 2a details primer placement) **F)** Coding potential analysis assessed via the Coding-potential Assessment Tool including *miR34a* asRNA, two characterized non-coding RNA transcripts (*HOTAIR* and *XIST*), and three known protein-coding transcripts (β -actin, tubulin, and *MYC*).

141
142 We next sought to interrogate primary cancer samples to examine if a
143 correlation between *miR34a* asRNA and *miR34a* expression levels could be
144 identified. For this task we utilized RNA sequencing data from The Cancer
145 Genome Atlas (TCGA) after stratifying patients by cancer type, *TP53* status
146 and, where appropriate, cancer subtypes. The results indicate
147 that *miR34a* asRNA and *miR34a* expression are strongly correlated in the
148 vast majority of cancer types examined, both in the presence and absence of
149 wild-type *TP53* (**Fig. 1c, Figure 1-Figure Supplement 1a**). The results also
150 further confirm that the expression levels of both *miR34a* and its asRNA tend
151 to be reduced in patients with nonsynonymous *TP53* mutations (**Figure 1-**
152 **Figure Supplement 1b**).

153
154 Next, we aimed to gain a thorough understanding of *miR34a* asRNA's
155 molecular characteristics and cellular localization. To experimentally
156 determine the 3' termination site for the *miR34a* asRNA transcript we
157 performed 3' rapid amplification of cDNA ends (RACE) using the U2OS
158 osteosarcoma cell line that exhibited high endogenous levels
159 of *miR34a* asRNA in the cell panel screening. By sequencing the cloned
160 cDNA we determined that the transcripts 3' transcription termination site is
161 525 base pairs upstream of the *LINC01759* transcript's annotated termination
162 site (**Fig. 1d**). Next, we characterized the *miR34a* asRNA 5' transcription start
163 site by carrying out a primer walk assay, i.e. a common reverse primer was
164 placed in exon 2 and forward primers were gradually staggered upstream of
165 the transcripts annotated start site (**Figure 1-Figure Supplement 2a**). Our
166 results indicated that the 5' start site for *miR34a* asRNA is in fact

167 approximately 90bp (F11 primer) to 220bp (F12 primer) upstream of the
168 annotated start site (**Fig. 1e**). Polyadenylation status was evaluated via cDNA
169 synthesis with either random nanomers or oligoDT primers followed by semi-
170 quantitative PCR with results indicating that the *miR34a* asRNA is
171 polyadenylated although the unspliced form seems to only be in the polyA
172 negative state (**Figure 1-Figure Supplement 2b**). We furthermore
173 investigated the propensity of *miR34a* asRNA to be alternatively spliced,
174 using PCR cloning and sequencing and found that the transcript is post-
175 transcriptionally spliced to form multiple different isoforms (**Figure 1-Figure**
176 **Supplement 2c**). ***make an additional supplementary figure showing spliced
177 RNAseq reads*** Finally, to evaluate the cellular localization of *miR34a*
178 asRNA we utilized RNA sequencing data from five cancer cell lines included
179 in the ENCODE (Consortium 2012) project that had been fractionated into
180 cytosolic and nuclear fractions. The analysis revealed that the *miR34a* asRNA
181 transcript localizes to both the nucleus and cytoplasm but primarily resides in
182 the nucleus (**Figure 1-Figure Supplement 2d**).

183

184 Finally, we utilized multiple approaches to evaluate the coding potential of
185 the *miR34a* asRNA transcript. The Coding-Potential Assessment Tool is a
186 bioinformatics-based tool that uses a logistic regression model to evaluate
187 coding-potential by examining ORF length, ORF coverage, Fickett score and
188 hexamer score (Wang et al. 2013). Results indicated that *miR34a* asRNA has
189 a similar lack of coding capacity to the known non-coding
190 transcripts *HOTAIR* and *XIST* and differs greatly when examining these
191 parameters to the known coding transcripts β -actin, tubulin, and *MYC* (**Fig.**

192 **1F).** We further confirmed these results using the Coding-Potential Calculator
193 that utilizes a support based machine-based classifier and accesses an
194 alternate set of discriminatory features (**Figure 1-Figure Supplement 2e**)
195 (Kong et al. 2007). *** We hope to be able to scan for peptides matching to
196 miR34a asRNA in CPTAC and Geiger et al., 2012 before submission and will
197 mention results here....***

198

199 **TP53-mediated regulation of *miR34a* asRNA expression**

200 *miR34a* is a known downstream target of TP53 and has been previously
201 shown to exhibit increased expression within multiple contexts of cellular
202 stress. *miR34a* asRNA has also been shown to be induced upon TP53
203 activation in several global analyses of p53-regulated lncRNAs (Rashi-Elkeles
204 et al. 2014, Hunten et al. 2015, Leveille et al. 2015, Ashouri et al. 2016, Kim et
205 al. 2017). To confirm these results in our biological system, we treated
206 HEK293t, embryonic kidney cells, and HCT116, colorectal cancer cells, with
207 the DNA damaging agent doxorubicin to activate TP53. QPCR-mediated
208 measurement of both *miR34a* HG and asRNA indicated that their expression
209 levels were increased in response to doxorubicin treatment in both cell lines
210 (**Fig. 2a**). To assess if it is in fact *TP53* that is responsible for the increase
211 in *miR34a* asRNA expression upon DNA damage, we
212 treated *TP53*^{+/+} and *TP53*^{-/-} HCT116 cells with increasing concentrations of
213 doxorubicin and monitored the expression of both *miR34a* HG and asRNA.
214 We observed a dose-dependent increase in both *miR34a* HG and asRNA
215 expression levels with increasing amounts of doxorubicin, indicating that
216 these two transcripts are co-regulated, although, this effect was largely

217 abrogated in TP53^{-/-} cells (**Fig. 2b**). These results indicate
218 that *TP53* activation increases *miR34a* asRNA expression upon the induction
219 of DNA damage. Nevertheless, *TP53*^{-/-} cells also showed a dose dependent
220 increase in both *miR34a* HG and asRNA, indicating that additional factors,
221 other than *TP53*, are capable of initiating an increase in expression of both of
222 these transcripts upon DNA damage.

223

224
225
226
227
228
229
230
231
232
233
234
235
236
237
238

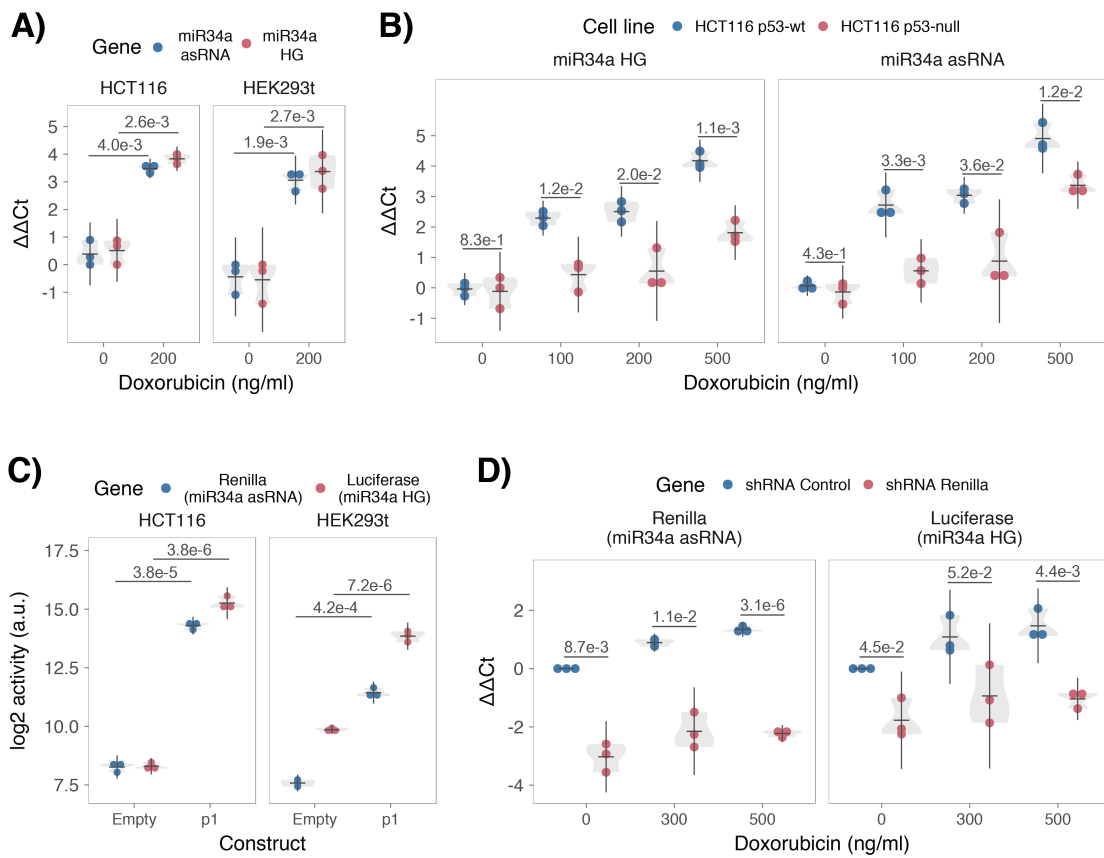


Figure 2: TP53-mediated regulation of the *miR34a* locus. **A)** Evaluating the effects of 24 hours of treatment with 200 ng/ml doxorubicin on *miR34a*asRNA and HG in HCT116 and HEK293t cells.* **B)** Monitoring *miR34a* HG and asRNA expression levels during 24 hours doxorubicin treatment in *TP53*^{+/+} and *TP53*^{-/-} HCT116 cells.* **C)** Quantification of luciferase and renilla levels after transfection of HCT116 and HEK293T cells with the p1 construct (See Figure 2 Supplement 2 for a schematic representation of the p1 construct).* **D)** HCT116 cells were co-transfected with the p1 construct and shRNA renilla or shRNA control and subsequently treated with increasing doses of doxorubicin. 24 hours post-treatment, cells were harvested and renilla and luciferase levels were measured using QPCR. Resulting p-values from statistical testing are shown above the shRenilla samples which were compared to the shRNA control using the respective treatment condition.* Individual points represent results from independent experiments and the gray shadow indicates the density of those points. Error bars show the 95% CI, black horizontal lines represent the mean, and p-values are shown over long horizontal lines indicating the comparison tested.

239 The head-to head orientation of *miR34a* HG and asRNA, suggests that
240 transcription is initiated from a single promoter in a bi-directional manner. To
241 investigate whether *miR34a* HG and asRNA are transcribed from the same
242 promoter as divergent transcripts, we cloned the *miR34a* HG promoter,
243 including the *TP53* binding site, into a luciferase/renilla dual reporter vector
244 which we hereafter refer to as p1 (**Figure 2-Figure Supplement 1a-b**). Upon
245 transfection of p1 into HCT116 and HEK293t cell lines we observed increases
246 in both luciferase and renilla indicating that *miR34a* HG and asRNA
247 expression can be regulated by a single promoter contained within the p1
248 construct (**Fig. 2c**).

249

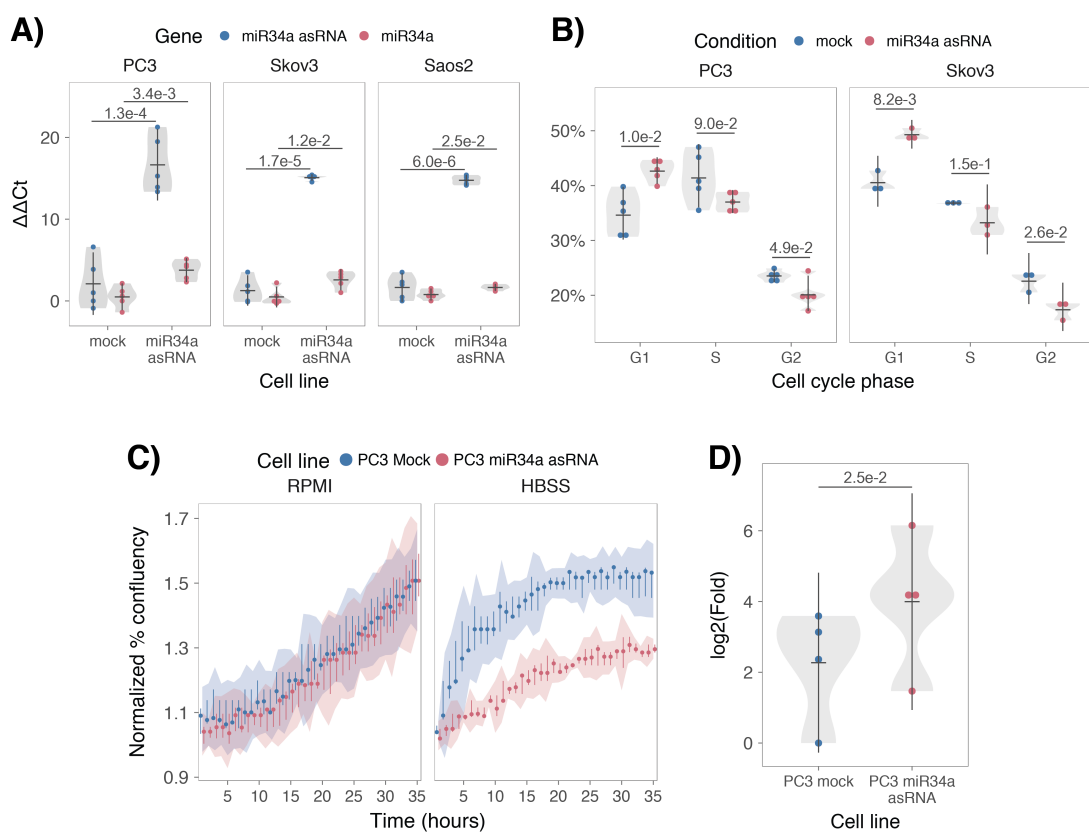
250 We hypothesized that *miR34a* asRNA may regulate *miR34a* HG levels and, in
251 addition, that the overlapping regions of the sense and antisense transcripts
252 may have a crucial role in mediating this regulation. Knock-down of
253 endogenous *miR34a* asRNA is complicated by its various isoforms (**Figure 1-**
254 **Figure Supplement 2c**). For this reason, we utilized the p1 construct to
255 evaluate the regulatory role of the miR34a asRNA on miR34a HG.
256 Accordingly, we first co-transfected the p1 construct, containing the
257 overlapping region of the two transcripts, and two different short hairpin (sh)
258 RNAs targeting renilla into HEK293T cells and subsequently measured
259 luciferase and renilla expression. The results indicated that shRNA-mediated
260 knock down of the p1-renilla transcript (corresponding to *miR34a* asRNA)
261 caused p1-luciferase (corresponding to *miR34a* HG) levels to concomitantly
262 decrease (**Figure 2-Figure Supplement 2**). These results indicate
263 that *miR34a* asRNA positively regulates levels of *miR34a* HG and that the

264 transcriptional product of the *miR34a* asRNA within in the p1 construct
265 promotes a miR34a response. To further support these conclusions and
266 better understand the role of miR34a asRNA during TP53 activation, *TP53*^{+/+}
267 HCT116 cells were co-transfected with p1 and shRNA renilla (2.1) and
268 subsequently treated with increasing doses of doxorubicin. Again, the results
269 showed a concomitant reduction in luciferase levels upon knock-down of p1-
270 renilla i.e. the *miR34a* asRNA corresponding segment of the p1 transcript
271 (**Fig. 2d**). Furthermore, the results showed that in the absence of p1-renilla
272 the expected induction of p1-luciferase in response to TP53 activation to DNA
273 damage is abrogated. Collectively these results indicate that *miR34a* asRNA
274 positively regulates miR34a expression and is crucial for an appropriate
275 TP53-mediated *miR34a* response to DNA damage.

276

277 ***miR34a* asRNA regulates its host gene independently of *TP53***
278 Despite the fact that TP53 regulates *miR34a* HG and asRNA expression, our
279 results indicated that other factors are also able to regulate this locus (**Fig.**
280 **2b**). Utilizing a lentiviral system, we stably over-expressed the *miR34a* asRNA
281 transcript in three *TP53*-null cell lines, PC3 (prostate cancer), Saos2
282 (osteogenic sarcoma), and Skov3 (adenocarcinoma). We first analyzed the
283 levels of *miR34a* asRNA in these stable over-expression cell lines, compared
284 to HEK293T cells, which have high endogenous levels of *miR34a* asRNA,
285 finding that, on average, the over-expression was approximately 30-fold
286 higher in the over-expression cell lines than in HEK293t cells. Due to the fact
287 that *miR34a* asRNA can be up-regulated ~30-fold in response to DNA
288 damage (**Fig. 2b**), we deemed this over-expression level to correspond to

289 physiologically relevant levels in cells encountering a stress stimulus, such as
 290 DNA damage (**Figure 3-Figure Supplement 1**). Analysis of *miR34a* levels in
 291 the *miR34a* asRNA over-expressing cell lines showed that *miR34a* asRNA
 292 over-expression resulted in a concomitant increase in the expression
 293 of *miR34a* in all three cell lines (**Fig. 3a**). These results indicate that, in the
 294 absence of *TP53*, *miR34a* expression may be rescued by increasing the
 295 levels of *miR34a* asRNA expression.



296

297 **Figure 3: miR34a asRNA positively regulates miR34a and its associated phenotypes.** **A)** QPCR-
 298 mediated quantification of *miR34a* expression in cell lines stably over-
 299 expressing *miR34a* asRNA.* **B)** Cell cycle analysis comparing stably over-expressing *miR34a* asRNA
 300 cells to the respective mock expressing cells.* **C)** Analysis of cellular growth over time in *miR34a*
 301 asRNA over-expressing PC3 cells. Points represent the median from 3 independent experiments, the
 302 colored shadows indicate the 95% confidence interval, and vertical lines show the minimum and
 303 maximum values obtained from the three biological replicates. **D)** Differential phosphorylated
 304 polymerase II binding in *miR34a* asRNA over-expressing PC3 cells.* Individual points represent
 305 results from independent experiments and the gray shadow indicates the density of those points. Error
 306 bars show the 95% CI, black horizontal lines represent the mean, and p-values are shown over long
 307 horizontal lines indicating the comparison tested.
 308

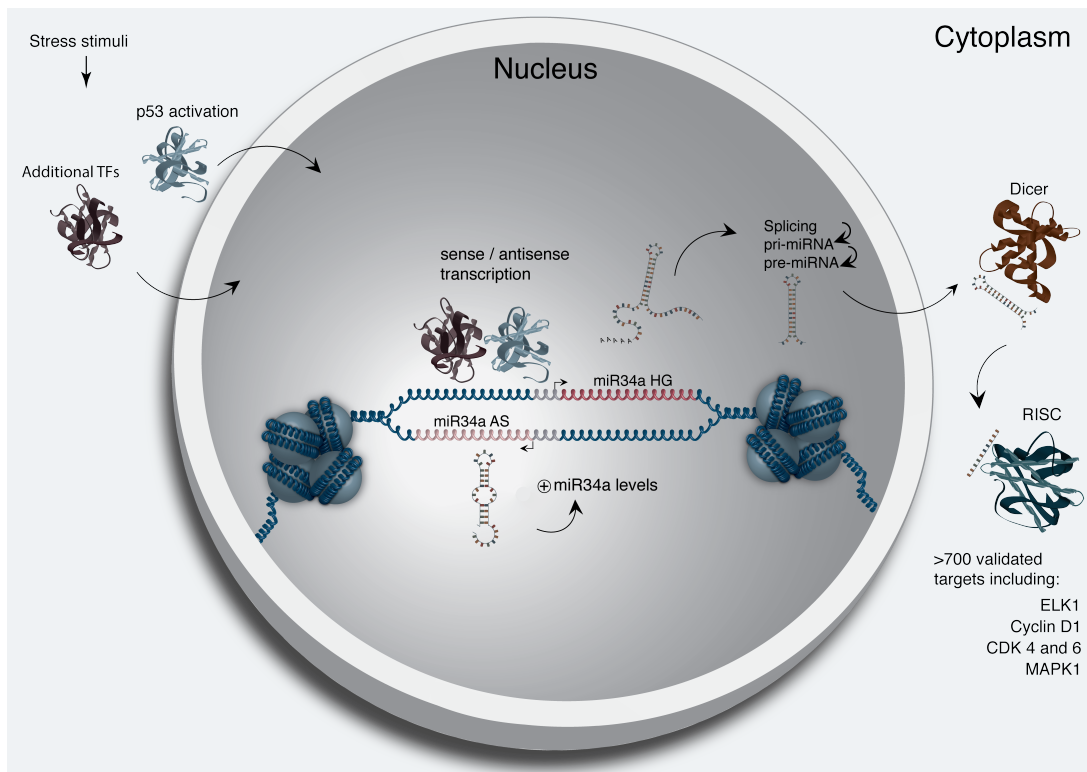
309 *miR34a* has been previously shown to regulate cell cycle progression, with
310 *miR34a* induction causing G1 arrest. Cell cycle analysis via determination of
311 DNA content showed a significant increase in G1 phase cells in the PC3 and
312 Skov3 *miR34a* asRNA over-expressing cell lines, indicative of G1 arrest, as
313 well as, a significant decrease of cells in G2 phase (**Fig. 3b**). *miR34a*'s effects
314 on the cell cycle are mediated by its ability to target cell cycle regulators such
315 as cyclin D1 (*CCND1*) (Sun et al. 2008). We therefore sought to determine if
316 the *miR34a* asRNA over-expressing cell lines exhibited effects on this
317 known *miR34a* target. Quantification of both *CCND1* RNA expression (**Figure**
318 **3-Figure Supplement 2a**) and protein levels (**Figure 3-Figure Supplement**
319 **2b**) in the PC3 *miR34a* asRNA over-expressing cell line showed a significant
320 decrease of *CCND1* levels compared to the mock control.

321
322 *miR34a* is also a well known inhibitor of cellular growth via its ability to
323 regulate growth factor signaling. Furthermore, starvation has been shown to
324 induce *miR34a* expression that down-regulates multiple targets that aid in the
325 phosphorylation of multiple pro-survival growth factors (Lal et al. 2011). We
326 further interrogated the effects of *miR34a* asRNA over-expression by
327 investigating the growth of the cells in both normal and starvation conditions
328 by measuring confluency over a 35-hour period. Under normal growth
329 conditions there is a small but significant reduction ($p = 3.0e-8$) in confluency
330 in the *miR34a* asRNA over-expressing cell lines, these effects on cell growth
331 are drastically increased in starvation conditions ($p = 9.5e-67$). This is in
332 accordance with our previous results, and suggests that *miR34a* asRNA-
333 mediated increases in *miR34a* expression are crucial under conditions of

334 stress and necessary for the initiation of an appropriate cellular response. In
335 summary, we find that over-expression of *miR34a* asRNA is sufficient to
336 increase *miR34a* expression and gives rise to known phenotypes observed
337 with increased *miR34a* expression.

338

339 Antisense RNAs have been reported to mediate their effects both via
340 transcriptional and post-transcriptional mechanisms. Due to the fact that
341 *miR34a* expression is undetected in wild type PC3 cells but, upon over-
342 expression of *miR34a* asRNA, increases to detectable levels, we
343 hypothesized that *miR34a* asRNA is capable of regulating *miR34a* expression
344 levels via a transcriptional mechanism. To ascertain if this is actually the case,
345 we performed chromatin immunoprecipitation (ChIP) for phosphorylated
346 polymerase II (polII) at the *miR34a* HG promoter in both *miR34a* asRNA over-
347 expressing and mock control cell lines. Our results indicated a clear increase
348 in phosphorylated polII binding at the *miR34a* promoter upon *miR34a* asRNA
349 over-expression indicating *miR34a* asRNA's ability to regulate *miR34a* levels
350 on a transcriptional level (**Fig. 3d**).



351

352 **Figure 4: A graphical summary of the proposed *miR34a* asRNA function.** Stress stimuli,
 353 originating in the cytoplasm or nucleus, activates *TP53* as well as additional factors. These factors then
 354 bind to the *miR34a* promoter and drive transcription of the sense and antisense strands. *miR34a* asRNA
 355 serves to increase the levels of *miR34a* HG transcription via an unknown mechanism. *miR34a* HG
 356 then, in turn, is then spliced, processed by the RNase III enzyme Drosha, and exported to the
 357 cytoplasm. The *miR34a* pre-miRNA then binds to Dicer where the hair-pin loop is cleaved and
 358 mature *miR34a* is formed. Binding of the mature *miR34a* miRNA to the RISC complex then allows it
 359 to bind and repress its targets.
 360

361 ***You can add polII in this figure***

362 **Discussion**

363
364 Multiple studies have previously shown asRNAs to be crucial for the
365 appropriate regulation of cancer-associated protein-coding genes and that
366 their dys-regulation can lead to perturbation of tumor suppressive and
367 oncogenic pathways, as well as, cancer-related phenotypes (Yu et al. 2008,
368 Yap et al. 2010, Serviss et al. 2014, Balbin et al. 2015). Here we show that
369 asRNAs are also capable of regulating cancer-associated miRNAs resulting in
370 similar consequences as protein-coding gene dys-regulation (**Fig. 4**).
371 Interestingly, we show that, both in the presence and absence of
372 *TP53*, *miR34a* asRNA provides an additional regulatory level and functions by
373 mediating the increase of *miR34a* expression in both homeostasis and upon
374 encountering multiple forms of cellular stress. Furthermore, we find that
375 *miR34a* asRNA-mediated increases in *miR34a* expression levels are sufficient
376 to drive the appropriate cellular responses to multiple forms of stress stimuli
377 that are encountered (**Fig. 2d and Fig. 3c**). Previous studies have utilized
378 various molecular biology methods to up regulate *miR34a* expression in a p53
379 deficient background showing similar phenotypic outcomes but, to our
380 knowledge, this is the first example of an endogenous mechanism by which
381 this can be achieved (Liu et al. 2011, Ahn et al. 2012, Yang et al. 2012,
382 Stahlhut et al. 2015, Wang et al. 2015).

383

384 In agreement with previous studies, we demonstrate that upon encountering
385 various types of cellular stress, TP53 in concert with additional factors bind
386 and initiate transcription at the *miR34a* locus, thus increasing the levels of
387 *miR34a* and, in addition, *miR34a* asRNA. We hypothesize that *miR34a*

388 asRNA may form a positive feedback for *miR34a* expression whereby *miR34a*
389 serves as a scaffold for the recruitment of additional factors that
390 facilitate polymerase II-mediated transcription, thus, increasing the expression
391 of *miR34a* and driving the cell towards a reduction in growth factor signaling,
392 senescence, and eventually apoptosis. On the other hand, in cells without a
393 functional *TP53*, other factors, which typically act independently or in concert
394 with *TP53*, may initiate transcription of the *miR34a* locus. We believe that
395 *miR34a* asRNA could potentially be interacting directly with one of these
396 additional factors and recruiting it to the *miR34a* locus in order to drive
397 *miR34a* transcription. This is especially plausible due to head-to-head
398 orientation of the *miR34a* HG and asRNA, causing sequence complementarity
399 between the RNA and the promoter DNA. Previous reports have also
400 illustrated the ability of asRNAs to form hybrid DNA:RNA R-loops and, thus,
401 facilitate an open chromatin structure and the transcription of the sense gene
402 (Boque-Sastre et al. 2015). The fact that the p1 construct only contains a
403 small portion of the *miR34a* asRNA transcript indicates that this portion is
404 sufficient to give rise to at least a partial *miR34a* inducing response and
405 therefore, indicates that *miR34a* asRNA may be able to facilitate *miR34a*
406 expression independent of additional factors (**Fig 2d, Figure 2-Figure**
407 **Supplement 2a**). Nevertheless, further work will need to be performed to
408 ascertain the mechanism that is utilized in the case of *miR34a* asRNA.

409
410 An unannotated transcript, *Lnc34a*, arising from the antisense orientation of
411 the *miR34a* locus and with a transcription start site >250 bp upstream of the
412 annotated *miR34a* asRNAs start site, has been previously reported in a study

413 examining colorectal cancer (Wang et al. 2016). Among the findings in Wang
414 et al. the authors discover that *Lnc34a* negatively regulates miR34a
415 expression via recruitment of *DNMT3a*, *PHB2*, and *HDAC1* to the *miR34a*
416 promoter. Although the *Lnc34a* and *miR34a* asRNA transcripts share some
417 sequence similarity, we believe them to be separate RNAs that are,
418 potentially, different isoforms of the same gene. Furthermore, *Lnc34a* may be
419 highly context dependent and potentially only expressed at biologically
420 significant levels in colon cancer stem cells, or other stem-like cells, in
421 agreement with the conclusions drawn in the paper. We thoroughly address
422 our reasons for these beliefs and give appropriate supporting evidence in
423 (**Supplementary Results 4**). The fact that *Lnc34a* and *miR34a* asRNA would
424 appear to have opposing roles in their regulation of *miR34a* further underlines
425 the complexity of the regulation at this locus.

426

427 Clinical trials utilizing miR34a replacement therapy have previously been
428 conducted but, disappointingly, were terminated after adverse side effects of
429 an immunological nature were observed in several of the patients (Slabakova
430 et al. 2017). Although it is not presently clear if these side effects were caused
431 by *miR34a* or the liposomal carrier used to deliver the miRNA, the multitude of
432 evidence indicating *miR34a*'s crucial role in oncogenesis still makes its
433 therapeutic induction an interesting strategy for therapy and needs further
434 investigation. In summary, our results indicate that *miR34a* asRNA is a vital
435 player in the regulation of *miR34a* and is especially important typical
436 examples of cellular stress encountered in cancer. We believe the
437 conclusions drawn in this study to be essential in the progress towards

438 developing a better understanding of the regulation of cancer-associated
439 miRNAs and, specifically, the tumor suppressor miR34a.

440

441 **Materials and Methods**

442 **Cell Culture**

443 All cell lines were cultured at 5% CO₂ and 37° C with HEK293T, Saos2, and
444 Skov3 cells cultured in DMEM high glucose (GE Healthcare Life Sciences,
445 Hyclone, UT, USA, Cat# SH30081), HCT116 and U2OS cells in McCoy's 5a
446 (ThermoFisher Scientific, MA, USA, Cat# SH30200), and PC3 cells in RPMI
447 (GE Healthcare Life Sciences, Hyclone, Cat# SH3009602) and 2 mM L-
448 glutamine (GE Healthcare Life Sciences, Hyclone, Cat# SH3003402). All
449 growth mediums were supplemented with 10% heat-inactivated FBS
450 (ThermoFisher Scientific, Gibco, Cat# 12657029) and 50 µg/ml of
451 streptomycin (ThermoFisher Scientific, Gibco, Cat# 15140122) and 50 µg/ml
452 of penicillin (ThermoFisher Scientific, Gibco, Cat# 15140122).

453 454 **Bioinformatics and Data Availability**

455 The USCS genome browser (Kent et al. 2002) was utilized for the
456 bioinformatic evaluation of antisense transcription utilizing the RefSeq
457 (O'Leary et al. 2016) gene annotation track.

458

459 All raw experimental data, code used for analysis, and supplementary
460 methods are available for review at ([Serviss 2017](#)) and are provided as an R
461 package. All analysis took place using the R statistical programming language
462 (Team 2017) using multiple external packages that are all documented in the
463 package associated with the article (Wilkins , Chang 2014, Wickham 2014,

464 Wickham 2016, Allaire et al. 2017, Arnold 2017, Wickham 2017, Wickham
465 2017, Wickham 2017, Xiao 2017, Xie 2017). The package facilitates
466 replication of the operating system and package versions used for the original
467 analysis, reproduction of each individual figure included in the article, and
468 easy review of the code used for all steps of the analysis, from raw-data to
469 figure.

470

471 **Coding Potential**

472 Protein-coding capacity was evaluated using the Coding-potential
473 Assessment Tool (Wang et al. 2013) and Coding-potential Calculator (Kong et
474 al. 2007) with default settings. Transcript sequences for use with Coding-
475 potential Assessment Tool were downloaded from the UCSC genome
476 browser using the Ensembl
477 accessions: *HOTAIR* (ENST00000455246), *XIST* (ENST00000429829), β-
478 actin (ENST00000331789), Tubulin (ENST00000427480),
479 and *MYC* (ENST00000377970). Transcript sequences for use with Coding-
480 potential Calculator were downloaded from the UCSC genome browser using
481 the following IDs: *HOTAIR* (uc031qho.1), β-actin (uc003soq.4).

482

483 **shRNAs**

484 shRNA-expressing constructs were cloned into the U6M2 construct using the
485 BgIII and KpnI restriction sites as previously described (Amarzguioui et al.
486 2005). shRNA constructs were transfected using Lipofectamine 2000 or 3000
487 (ThermoFisher Scientific, Cat# 12566014 and L3000015). The sequences
488 targeting renilla is as follows: shRenilla 1.1 (AAT ACA CCG CGC TAC TGG

489 C), shRenilla 2.1 (TAA CGG GAT TTC ACG AGG C).

490

491 **Lentiviral Particle production, infection, and selection**

492 Lentivirus production was performed as previously described in (Turner et al.
493 2012). Briefly, HEK293T cells were transfected with viral and expression
494 constructs using Lipofectamine 2000 (ThermoFisher Scientific, Cat#
495 12566014), after which viral supernatants were harvested 48 and 72 hours
496 post-transfection. Viral particles were concentrated using PEG-IT solution
497 (Systems Biosciences, CA, USA, Cat# LV825A-1) according to the
498 manufacturer's recommendations. HEK293T cells were used for virus titration
499 and GFP expression was evaluated 72hrs post-infection via flow cytometry
500 (LSRII, BD Biosciences, CA, USA) after which TU/ml was calculated.

501

502 Stable lines were generated by infecting cells with a multiplicity of infection of
503 1 after which 1-2 µM mycophenolic acid (Merck, NJ, USA, Cat# M5255)
504 selection was initiated 48 hours post-infection. Cells were expanded as the
505 selection process was monitored via flow cytometry analysis (LSRII, BD
506 Biosciences) of GFP and selection was terminated once > 90% of the cells
507 were GFP positive.

508

509 **Western Blotting**

510 Samples were lysed in 50 mM Tris-HCl (Sigma Aldrich, MO, USA, Cat#
511 T2663), pH 7.4, 1% NP-40 (Sigma Aldrich, Cat# I8896), 150 mM NaCl (Sigma
512 Aldrich, Cat# S5886), 1 mM EDTA (Promega, WI, USA, Cat# V4231), 1%
513 glycerol (Sigma Aldrich, Cat# G5516), 100 µM vanadate (), protease inhibitor

514 cocktail (Roche Diagnostics, Basel, Switzerland, Cat# 004693159001) and
515 PhosSTOP (Roche Diagnostics, Cat# 04906837001). Lysates were subjected
516 to SDS-PAGE and transferred to PVDF membranes. The proteins were
517 detected by western blot analysis by using an enhanced chemiluminescence
518 system (Western Lightning–ECL, PerkinElmer, Cat# NEL103001EA).
519 Antibodies used were specific for CCND1 1:1000 (Cell Signaling, Cat# 2926),
520 and β-actin 1:5000 (Sigma-Aldrich, Cat# A5441). All western blot
521 quantifications were performed using ImageJ (Schneider et al. 2012).

522

523 **Generation of U6-expressed miR34a AS Lentiviral Constructs**

524 The U6 promoter was amplified from the U6M2 cloning plasmid (Amarzguioui
525 et al. 2005) and ligated into the Not1 restriction site of the pHIV7-IMPDH2
526 vector (Turner et al. 2012). miR43a asRNA was PCR amplified and
527 subsequently cloned into the Nhe1 and Pac1 restriction sites in the pHIV7-
528 IMPDH2-U6 plasmid.

529

530 **Promoter Activity**

531 Cells were co-transfected with the renilla/firefly bidirectional promoter
532 construct (Polson et al. 2011) and GFP by using Lipofectamine 2000 (Life
533 Technologies, Cat# 12566014). The expression of GFP and luminescence
534 was measured 24 h post transfection by using the Dual-Glo Luciferase Assay
535 System (Promega, Cat# E2920) and detected by the GloMax-Multi+ Detection
536 System (Promega, Cat# SA3030). The expression of luminescence was
537 normalized to GFP.

538

539 **RNA Extraction and cDNA Synthesis**

540 For downstream SYBR green applications, RNA was extracted using the
541 RNeasy mini kit (Qiagen, Venlo, Netherlands, Cat# 74106) and subsequently
542 treated with DNase (Ambion Turbo DNA-free, ThermoFisher Scientific, Cat#
543 AM1907). 500ng RNA was used for cDNA synthesis using MuMLV
544 (ThermoFisher Scientific, Cat# 28025013) and a 1:1 mix of oligo(dT) and
545 random nanomers.

546

547 For analysis of miRNA expression with Taqman, samples were isolated with
548 TRIzol reagent (ThermoFisher Scientific, Cat# 15596018) and further
549 processed with the miRNeasy kit (Qiagen, Cat# 74106). cDNA synthesis was
550 performed using the TaqMan MicroRNA Reverse Transcription Kit
551 (ThermoFisher Scientific, Cat# 4366597) using the corresponding oligos
552 according to the manufacturer's recommendations.

553

554 **QPCR and PCR**

555 PCR was performed using the KAPA2G Fast HotStart ReadyMix PCR Kit
556 (Kapa Biosystems, MA, USA, Cat# KK5601) with corresponding primers.
557 QPCR was carried out using KAPA 2G SYBRRGreen (Kapa Biosystems, Cat#
558 KK4602) using the Applied Biosystems 7900HT machine with the cycling
559 conditions: 95 °C for 3 min, 95 °C for 3 s, 60 °C for 30 s.

560

561 QPCR for miRNA expression analysis was performed according to the primer
562 probe set manufacturers recommendations (ThermoFisher Scientific) and
563 using the TaqMan Universal PCR Master Mix (ThermoFisher Scientific, Cat#

564 4304437) with the same cycling scheme as above. Primer and probe sets for
565 TaqMan were also purchased from ThermoFisher Scientific (Life
566 Technologies at time of purchase, TaqMan® MicroRNA Assay, hsa-miR-34a,
567 human, Cat# 4440887, Assay ID: 000426 and Control miRNA Assay, RNU48,
568 human, Cat# 4440887, Assay ID: 001006).

569

570 Primers for all PCR-based experiments are listed in **Supplementary**
571 **Document 2** and arranged by figure.

572

573 **Bi-directional Promoter Cloning**

574 The overlapping region (p1) corresponds with the sequence previously
575 published as the TP53 binding site in (Raver-Shapira et al. 2007) which we
576 synthesized and cloned into the pLucRluc construct (Polson et al. 2011).

577

578 **Cell Cycle Distribution**

579 Cells were washed in PBS and fixed in 4% paraformaldehyde at room
580 temperature overnight. Paraformaldehyde was removed, and cells were re-
581 suspended in 95% EtOH. The samples were then rehydrated in distilled
582 water, stained with DAPI and analyzed by flow cytometry on a LSRII (BD
583 Biosciences) machine. Resulting cell cycle phases were quantified using the
584 ModFit software (Verity Software House, ME, USA).

585

586 **3' Rapid Amplification of cDNA Ends**

587 3'-RACE was performed as described as previously in (Johnsson et al. 2013).
588 Briefly, U2OS cell RNA was polyA-tailed using yeast polyA polymerase

589 (ThermoFisher Scientific, Cat# 74225Z25KU) after which cDNA was
590 synthesized using oligo(dT) primers. Nested-PCR was performed first using a
591 forward primer in miR34a asRNA exon 1 and a tailed oligo(dT) primer
592 followed by a second PCR using an alternate miR34a asRNA exon 1 primer
593 and a reverse primer binding to the tail of the previously used oligo(dT)
594 primer. PCR products were gel purified and cloned the Strata Clone Kit
595 (Agilent Technologies, CA, USA, Cat# 240205), and sequenced.

596

597 **Chromatin Immunoprecipitation**

598 The ChIP was performed as previously described in (Johnsson et al. 2013)
599 with the following modifications. Cells were crosslinked in 1% formaldehyde
600 (Merck, Cat# 1040039025), quenched with 0.125M glycine (Sigma Aldrich,
601 Cat# G7126), and lysed in cell lysis buffer comprised of: 5mM PIPES (Sigma
602 Aldrich, Cat# 80635), 85mM KCL (Merck, Cat# 4936), 0.5% NP40 (Sigma
603 Aldrich, Cat# I8896), protease inhibitor (Roche Diagnostics, Cat#
604 004693159001). Samples were then sonicated in 50mM TRIS-HCL pH 8.0
605 (Sigma Aldrich, MO, USA, Cat# T2663) 10mM EDTA (Promega, WI, USA,
606 Cat# V4231), 1% SDS (ThermoFisher Scientific, Cat# AM9822), and protease
607 inhibitor (Roche Diagnostics, Cat# 004693159001) using a Bioruptor
608 Sonicator (Diagenode, NJ, USA). Samples were incubated over night at 4°C
609 with the *polII* antibody (Abcam, Cambridge, UK, Cat# ab5095) and
610 subsequently pulled down with Salmon Sperm DNA/Protein A Agarose
611 (Millipore, Cat# 16-157) beads. DNA was eluted in an elution buffer of 1%
612 SDS (ThermoFisher Scientific, Cat# AM9822) 100mM NaHCO3 (Sigma
613 Aldrich, Cat# 71631), followed by reverse crosslinking, RNaseA

614 (ThermoFisher Scientific, Cat# 1692412) and protease K (New England
615 Biolabs, MA, USA, Cat# P8107S) treatment. The DNA was eluted using
616 Qiagen PCR purification kit (Cat# 28106).

617

618 **Confluency Analysis**

619 Cells were incubated in the Spark Multimode Microplate (Tecan) reader for 48
620 hours at 37°C with 5% CO₂ in a humidity chamber. Confluency was
621 measured every hour using bright-field microscopy and the percentage of
622 confluency was reported via the plate reader's inbuilt algorithm. Percentage of
623 confluency was normalized to the control sample in each condition (shown in
624 figure) and then ranked. The rank was then used to construct a linear model of
625 the dependency of the rank on the time and cell lines variables for each
626 growth condition. Reported p-values are derived from the t-test, testing the
627 null hypothesis that the coefficient estimate of the cell line variable is equal to
628 0.

629

630 **Pharmacological Compounds**

631 Doxorubicin was purchased from Teva (cat. nr. 021361).

632

633 **Cellular Localization Analysis**

634 Quantified RNAseq data from 11 cell lines from the GRCh38 assembly was
635 downloaded from the ENCODE project database and quantifications for
636 miR34a asRNA (ENSG00000234546), GAPDH (ENSG00000111640), and
637 MALAT1 (ENSG00000251562) were extracted. Cell lines for which data was
638 downloaded include: A549, GM12878, HeLa-S3, HepG2, HT1080, K562

639 MCF-7, NCI-H460, SK-MEL-5, SK-N-DZ, SK-N-SH. Initial exploratory analysis
640 revealed that several cell lines should be removed from the analysis due to a)
641 a larger proportion of GAPDH in the nucleus than cytoplasm or b) variation of
642 miR34a asRNA expression is too large to draw conclusions, or c) they have
643 no or low (<6 TPM) miR34a asRNA expression. Furthermore, only
644 polyadenylated libraries were used in the final analysis, due to the fact that
645 the cellular compartment enrichment was improved in these samples. All
646 analyzed genes are reported to be polyadenylated. In addition, only samples
647 with 2 biological replicates were retained. For each cell type, gene, and
648 biological replicate the fraction of transcripts per million (TPM) in each cellular
649 compartment was calculated as the fraction of TPM in the specific
650 compartment by the total TPM. The mean and standard deviation for the
651 fraction was subsequently calculated for each cell type and cellular
652 compartment and this information was represented in the final figure.

653

654 **CAGE Analysis**

655 All available CAGE data from the ENCODE project (Consortium 2012) for 36
656 cell lines was downloaded from the UCSC genome browser (Kent et al. 2002)
657 for genome version hg19. Of these, 28 cell lines had CAGE transcription start
658 sites (TSS) mapping to the plus strand of chromosome 1 and in regions
659 corresponding to 200 base pairs upstream of the *lnc34a* start site (9241796 -
660 200) and 200 base pairs upstream of the GENCODE
661 annotated *miR34a* asRNA start site (9242263 + 200). These cell lines
662 included: HFDPC, H1-hESC, HMEpC, HAoEC, HPIEpC, HSaVEC, GM12878,
663 hMSC-BM, HUVEC, AG04450, hMSC-UC, IMR90, NHDF, SK-N-SH_RA, BJ,

664 HOB, HPC-PL, HAoAF, NHEK, HVMF, HWP, MCF-7, HepG2, hMSC-AT,
665 NHEM.f_M2, SkMC, NHEM_M2, and HCH. In total 74 samples were included.
666 17 samples were polyA-, 47 samples were polyA+, and 10 samples were total
667 RNA. In addition, 34 samples were whole cell, 15 enriched for the cytosolic
668 fraction, 15 enriched for the nucleolus, and 15 enriched for the nucleus. All
669 CAGE transcription start sites were plotted and the RPKM of the individual
670 reads was used to color each read to indicate their relative abundance. In
671 cases where CAGE TSS spanned identical regions, the RPMKs of the regions
672 were summed and represented as one CAGE TSS in the figure. In addition, a
673 density plot shows the distribution of the CAGE reads in the specified
674 interval.

675

676 **Splice Junction Analysis**

677 All available whole cell (i.e. non-fractionated) spliced read data originating
678 from the Cold Spring Harbor Lab in the ENCODE project (Consortium 2012)
679 for 38 cell lines was downloaded from the UCSC genome browser (Kent et al.
680 2002). Of these cell lines, 36 had spliced reads mapping to the plus strand of
681 chromosome 1 and in the region between the *lnc34a* start (9241796) and
682 transcription termination (9257102) site (note that *miR34a* asRNA resides
683 totally within this region). Splice junctions from the following cell lines were
684 included in the final figure: A549, Ag04450, Bj, CD20, CD34 mobilized,
685 Gm12878, H1hesc, Haoaf, Haoec, Hch, Helas3, Hepg2, Hfdpc, Hmec,
686 Hmepc, Hmescat, Hmscbm, Hmscuc, Hob, Hpcpl, Hpiepc, Hsavec, Hsmm,
687 Huvec, Hvmf, Hwp, Imr90, Mcf7, Monocd14, Nhdf, Nhek, Nhemfm2,
688 Nhemm2, Nhlf, Skmc, and Sknsh. All splice junctions were included in the

689 figure and colored according to the number of reads corresponding to each. In
690 cases where identical reads were detected multiple times, the read count was
691 summed and represented as one read in the figure.

692

693 **Correlation analysis**

694 Erik/Jimmy should probably take this.

695

696 **Acknowledgments**

697

698 **Competing Interests**

699

700 The authors declare no competing interests.

701

702 **Figure Supplements**

703

704 List figure supplements here!

705

706 **Supplementary Figures**

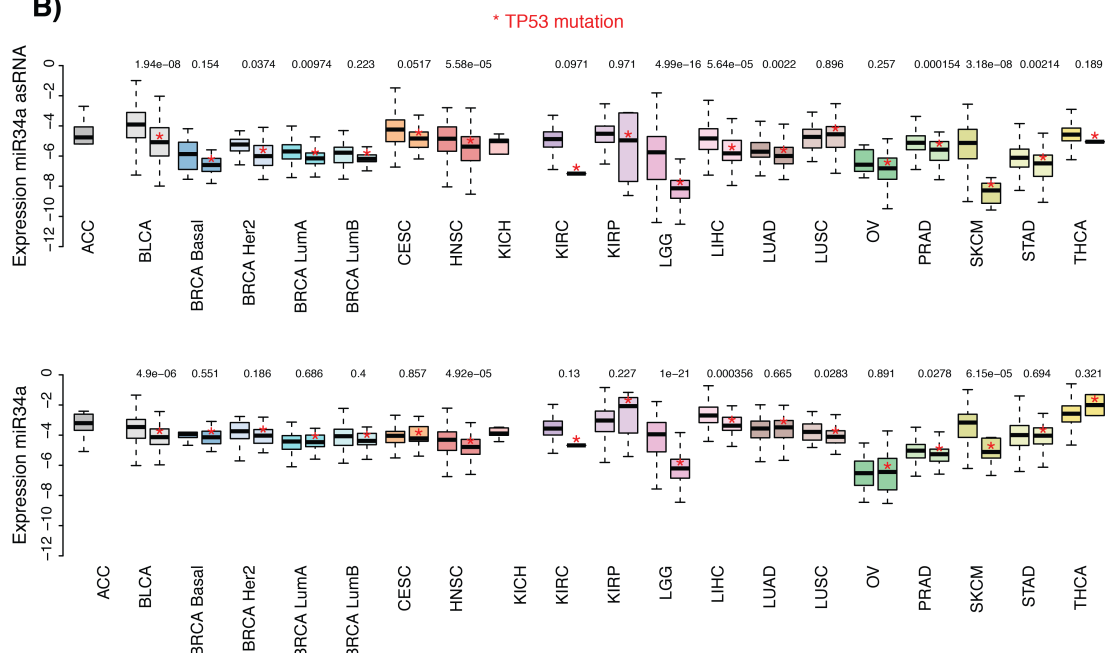
707

708

A)

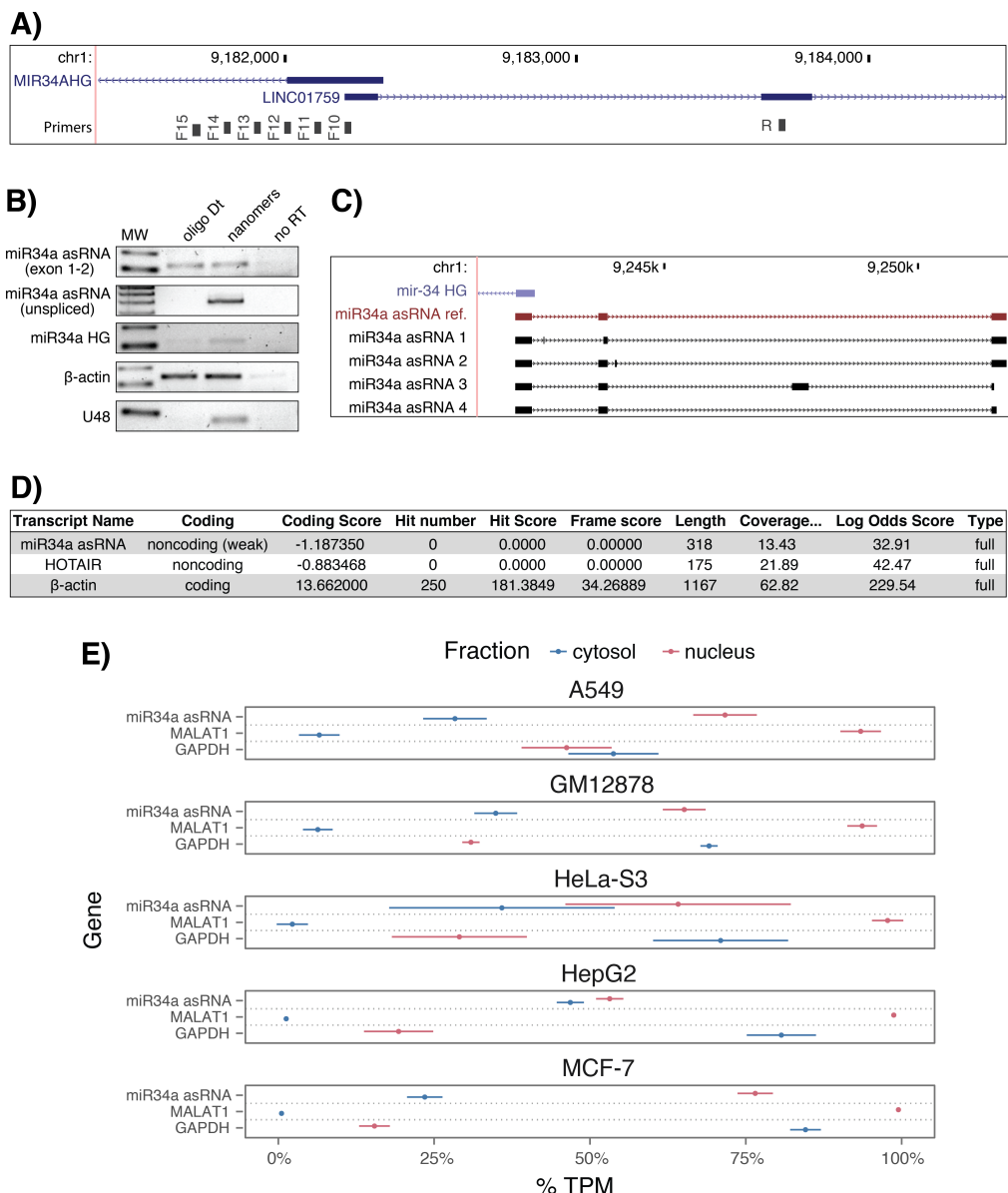
cancer	all n	all rho	all p	TP53wt n	TP53wt rho	TP53wt p	TP53mut n	TP53mut rho	TP53mut p
ACC	10	5.52e-01	1.04e-01	10	5.52e-01	1.04e-01	NA	NA	NA
BLCA	228	5.15e-01	7.89e-17	134	4.53e-01	3.86e-08	94	4.27e-01	1.73e-05
BRCA Basal	42	5.74e-01	9.54e-05	10	6.24e-01	6.02e-02	32	5.74e-01	7.41e-04
BRCA Her2	44	1.47e-01	3.39e-01	12	2.24e-01	4.85e-01	32	6.82e-02	7.10e-01
BRCA LumA	199	3.41e-01	8.22e-07	177	3.43e-01	2.96e-06	22	4.86e-01	2.31e-02
BRCA LumB	70	1.71e-01	1.57e-01	61	1.48e-01	2.53e-01	9	1.67e-01	6.78e-01
CESC	156	1.39e-01	8.37e-02	145	1.60e-01	5.45e-02	11	-4.55e-02	9.03e-01
HNSC	313	5.37e-01	8.38e-25	123	6.08e-01	0.00e+00	190	4.47e-01	9.68e-11
KICH	5	6.00e-01	3.50e-01	5	6.00e-01	3.50e-01	NA	NA	NA
KIRC	142	3.49e-01	2.06e-05	141	3.37e-01	4.41e-05	NA	NA	NA
KIRP	167	4.51e-01	9.16e-10	163	4.48e-01	2.04e-09	4	8.00e-01	3.33e-01
LGG	271	6.33e-01	9.92e-32	76	7.28e-01	0.00e+00	195	3.87e-01	2.26e-08
LIHC	153	5.63e-01	3.64e-14	114	5.16e-01	4.18e-09	39	4.55e-01	3.95e-03
LUAD	234	2.82e-01	1.15e-05	128	3.61e-01	2.87e-05	106	2.27e-01	1.91e-02
LUSC	139	2.29e-01	6.74e-03	42	4.17e-02	7.93e-01	97	3.29e-01	9.91e-04
OV	56	2.33e-01	8.37e-02	10	8.42e-01	4.46e-03	46	1.46e-01	3.31e-01
PRAD	413	4.66e-01	1.33e-23	375	4.59e-01	6.13e-21	38	4.50e-01	4.58e-03
SKCM	165	6.48e-01	5.43e-21	152	6.10e-01	7.85e-17	13	4.34e-01	1.40e-01
STAD	225	3.72e-01	8.23e-09	145	3.67e-01	5.71e-06	80	4.20e-01	1.03e-04
THCA	469	4.58e-01	1.07e-25	467	4.62e-01	4.06e-26	NA	NA	NA

B)



709
710
711
712
713
714
715
716
717
718
719

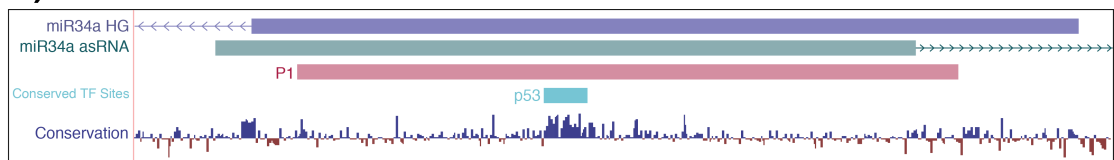
Figure 1 Supplement 1: TCAG Correlation analysis statistics. A) Spearman's rho and p-values (p) from the correlation analysis investigating the correlation between miR34a and miR34a asRNA expression in TP53 wild type (wt) and mutated (mut) samples within TCGA cancer types. B) Expression levels of miR34a and miR34a asRNA in TP53 wt and nonsynonymous mutation samples. Bladder Urothelial Carcinoma (BLCA), Breast invasive carcinoma (BRCA), Head and Neck squamous cell carcinoma (HNSC), Lower Grade Glioma (LGG), Liver hepatocellular carcinoma (LIHC), Lung adenocarcinoma (LUAD), Lung squamous cell carcinoma (LUSC), Ovarian serous cystadenocarcinoma (OV), Prostate adenocarcinoma (PRAD), Skin Cutaneous Melanoma (SKCM), Stomach adenocarcinoma (STAD).



720
721
722
723
724
725
726
727
728
729
730
731
732

Figure 1 Supplement 2: Molecular characteristics of miR34a asRNA. **A)** A schematic representation of the primer placement in the primer walk assay. **B)** Polyadenylation status of spliced and unspliced miR34a asRNA in HEK293T cells. **C)** Sequencing results from the analysis of *miR34a* asRNA isoforms in U2OS cells. *miR34a* AS ref. refers to the full length transcript as defined by the 3'-RACE and primer walk assay. **D)** Analysis of coding potential of the *miR34a* asRNA transcript using the Coding-potential Calculator. **E)** RNAseq data from five fractionated cell lines in the ENCODE project showing the percentage of transcripts per million (TPM) for miR34a asRNA. MALAT1 (nuclear localization) and GAPDH (cytoplasmic localization) are included as fractionation controls. Points represent the mean and horizontal lines represent the standard deviation from two biological replicates.

A)

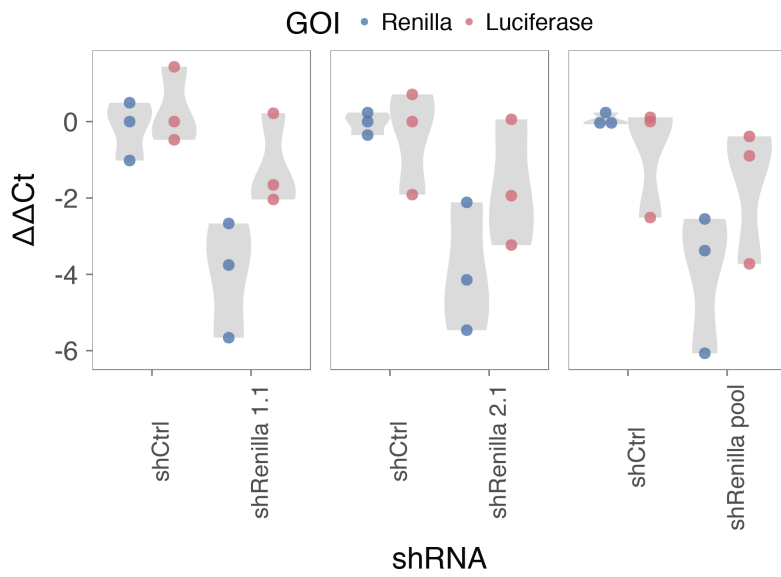


B)



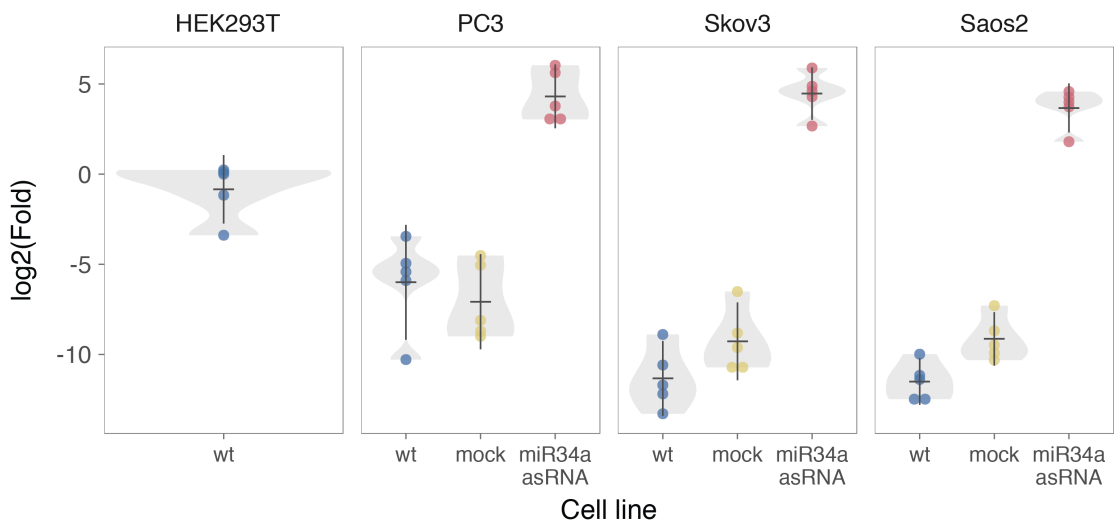
733
734
735
736
737
738

Figure 2 Supplement 1: A schematic representation of the p1 construct. A) A UCSC genome browser illustration indicating the location of the promoter region cloned into the p1 construct including the conserved *TP53*-binding site. **B)** A representative picture of the p1 construct including forward (F) and reverse (R) primer locations and the renilla shRNA targeting site.



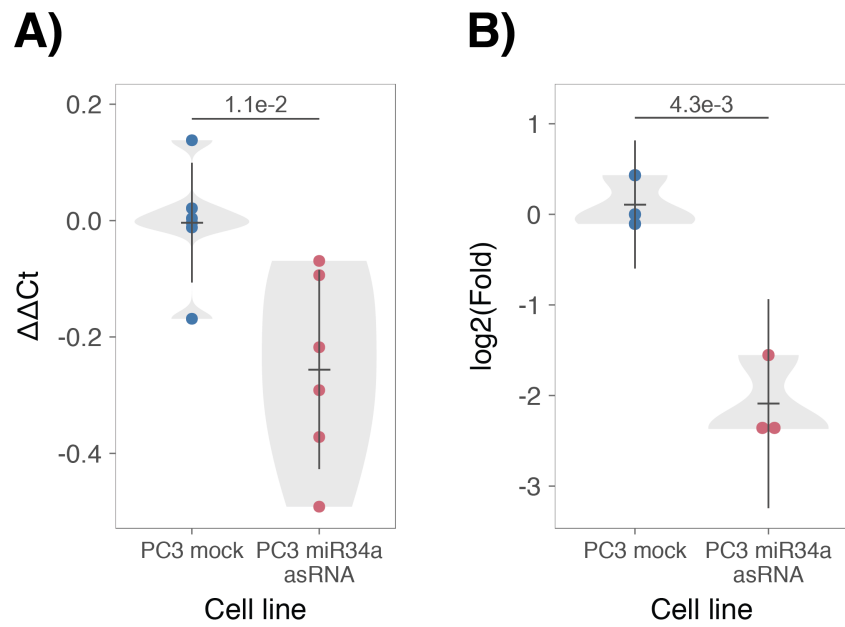
739
740
741
742
743
744

Figure 2 Supplement 2: miR34a HG response to p1-renilla knock-down. HEK293T cells were co-transfected with the P1 construct and either shRenilla or shControl. Renilla and luciferase levels were measured with Q-PCR 48 hours after transfection. Individual points represent independent experiments with the gray shadow indicating the density of the points.



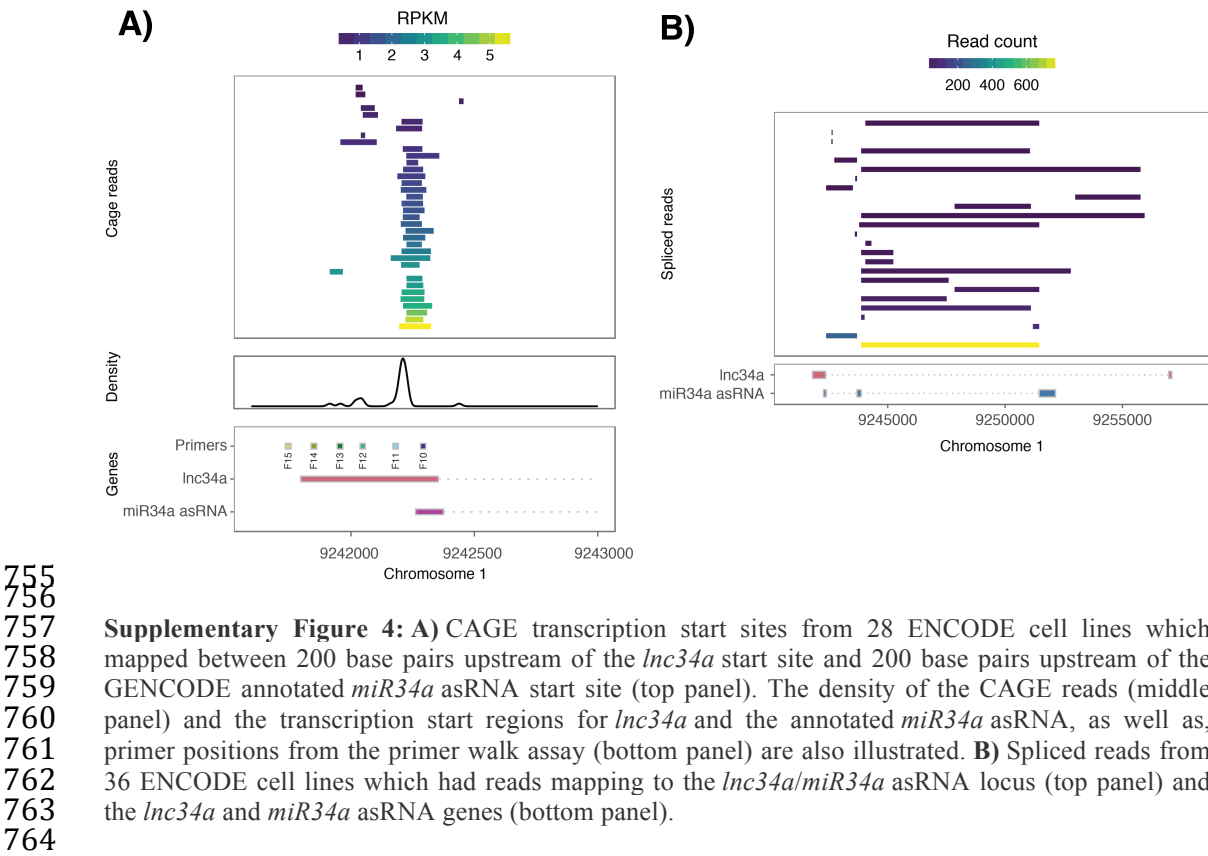
745
746

747 **Figure 3 Supplement 1: Physiological relevance of *miR34a* asRNA overexpression.** Comparison
748 of *miR34a* asRNA expression in HEK293T cells (high endogenous *miR34a* asRNA), and the wild-type
749 (wt), mock, and *miR34a* asRNA over-expressing stable cell lines.



750
751
752
753
754

Figure 3 Supplement 2: Effects of miR34a asRNA overexpression on CCND1. CCND1 expression (A) and western blot quantification of protein levels (B) in *miR34a* asRNA over-expressing PC3 stable cell lines.



765

766 References

767

768 Agostini, M., P. Tucci, R. Killick, E. Candi, B. S. Sayan, P. Rivetti di Val Cervo, P.
 769 Nicotera, F. McKeon, R. A. Knight, T. W. Mak and G. Melino (2011). "Neuronal
 770 differentiation by TAp73 is mediated by microRNA-34a regulation of synaptic
 771 protein targets." *Proc Natl Acad Sci U S A* **108**(52): 21093-21098. DOI:
 772 10.1073/pnas.1112061109

773

774 Ahn, Y. H., D. L. Gibbons, D. Chakravarti, C. J. Creighton, Z. H. Rizvi, H. P. Adams, A.
 775 Pertsemlidis, P. A. Gregory, J. A. Wright, G. J. Goodall, E. R. Flores and J. M. Kurie
 776 (2012). "ZEB1 drives prometastatic actin cytoskeletal remodeling by
 777 downregulating miR-34a expression." *J Clin Invest* **122**(9): 3170-3183. DOI:
 778 10.1172/JCI63608

779

780 Allaire, J., Y. Xie, J. McPherson, J. Luraschi, K. Ushey, A. Atkins, H. Wickham, J.
 781 Cheng and W. Chang (2017). rmarkdown: Dynamic Documents for R. R package
 782 version 1.8. <https://CRAN.R-project.org/package=rmarkdown>

783

784 Amarzguioui, M., J. J. Rossi and D. Kim (2005). "Approaches for chemically
 785 synthesized siRNA and vector-mediated RNAi." *FEBS Lett* **579**(26): 5974-5981.
 786 DOI: 10.1016/j.febslet.2005.08.070

787

788 Arnold, J. B. (2017). ggthemes: Extra Themes, Scales and Geoms for 'ggplot2'. R
 789 package version 3.4.0. <https://CRAN.R-project.org/package=ggthemes>

790

791 Ashouri, A., V. I. Sayin, J. Van den Eynden, S. X. Singh, T. Papagiannakopoulos and
 792 E. Larsson (2016). "Pan-cancer transcriptomic analysis associates long non-
 793 coding RNAs with key mutational driver events." *Nature Communications* **7**:
 794 13197. DOI: 10.1038/ncomms13197

795

796 Balbin, O. A., R. Malik, S. M. Dhanasekaran, J. R. Prensner, X. Cao, Y. M. Wu, D.
 797 Robinson, R. Wang, G. Chen, D. G. Beer, A. I. Nesvizhskii and A. M. Chinnaian
 798 (2015). "The landscape of antisense gene expression in human cancers." *Genome
 799 Res* **25**(7): 1068-1079. DOI: 10.1101/gr.180596.114

800

801 Boque-Sastre, R., M. Soler, C. Oliveira-Mateos, A. Portela, C. Moutinho, S. Sayols, A.
 802 Villanueva, M. Esteller and S. Guil (2015). "Head-to-head antisense transcription
 803 and R-loop formation promotes transcriptional activation." *Proc Natl Acad Sci U
 804 S A* **112**(18): 5785-5790. DOI: 10.1073/pnas.1421197112

805

806 Chang, T. C., D. Yu, Y. S. Lee, E. A. Wentzel, D. E. Arking, K. M. West, C. V. Dang, A.
 807 Thomas-Tikhonenko and J. T. Mendell (2008). "Widespread microRNA
 808 repression by Myc contributes to tumorigenesis." *Nat Genet* **40**(1): 43-50. DOI:
 809 10.1038/ng.2007.30

810

811 Chang, W. (2014). extrafont: Tools for using fonts. R package version 0.17.
 812 <https://CRAN.R-project.org/package=extrafont>

813

- 814 Chen, J., M. Sun, W. J. Kent, X. Huang, H. Xie, W. Wang, G. Zhou, R. Z. Shi and J. D.
815 Rowley (2004). "Over 20% of human transcripts might form sense-antisense
816 pairs." *Nucleic Acids Res* **32**(16): 4812-4820. DOI: 10.1093/nar/gkh818
- 817
- 818 Cheng, J., L. Zhou, Q. F. Xie, H. Y. Xie, X. Y. Wei, F. Gao, C. Y. Xing, X. Xu, L. J. Li and S.
819 S. Zheng (2010). "The impact of miR-34a on protein output in hepatocellular
820 carcinoma HepG2 cells." *Proteomics* **10**(8): 1557-1572. DOI:
821 10.1002/pmic.200900646
- 822
- 823 Chim, C. S., K. Y. Wong, Y. Qi, F. Loong, W. L. Lam, L. G. Wong, D. Y. Jin, J. F. Costello
824 and R. Liang (2010). "Epigenetic inactivation of the miR-34a in hematological
825 malignancies." *Carcinogenesis* **31**(4): 745-750. DOI: 10.1093/carcin/bgq033
- 826
- 827 Cole, K. A., E. F. Attiyeh, Y. P. Mosse, M. J. Laquaglia, S. J. Diskin, G. M. Brodeur and
828 J. M. Maris (2008). "A functional screen identifies miR-34a as a candidate
829 neuroblastoma tumor suppressor gene." *Mol Cancer Res* **6**(5): 735-742. DOI:
830 10.1158/1541-7786.MCR-07-2102
- 831
- 832 Conley, A. B. and I. K. Jordan (2012). "Epigenetic regulation of human cis-natural
833 antisense transcripts." *Nucleic Acids Res* **40**(4): 1438-1445. DOI:
834 10.1093/nar/gkr1010
- 835
- 836 Consortium, E. P. (2012). "An integrated encyclopedia of DNA elements in the
837 human genome." *Nature* **489**(7414): 57-74. DOI: 10.1038/nature11247
- 838
- 839 Ding, N., H. Wu, T. Tao and E. Peng (2017). "NEAT1 regulates cell proliferation
840 and apoptosis of ovarian cancer by miR-34a-5p/BCL2." *Onco Targets Ther* **10**:
841 4905-4915. DOI: 10.2147/OTT.S142446
- 842
- 843 Djebali, S., C. A. Davis, A. Merkel, A. Dobin, T. Lassmann, A. Mortazavi, A. Tanzer, J.
844 Lagarde, W. Lin, F. Schlesinger, C. Xue, G. K. Marinov, J. Khatun, B. A. Williams, C.
845 Zaleski, J. Rozowsky, M. Roder, F. Kokocinski, R. F. Abdelhamid, T. Alioto, I.
846 Antoshechkin, M. T. Baer, N. S. Bar, P. Batut, K. Bell, I. Bell, S. Chakrabortty, X.
847 Chen, J. Chrast, J. Curado, T. Derrien, J. Drenkow, E. Dumais, J. Dumais, R.
848 Duttagupta, E. Falconnet, M. Fastuca, K. Fejes-Toth, P. Ferreira, S. Foissac, M. J.
849 Fullwood, H. Gao, D. Gonzalez, A. Gordon, H. Gunawardena, C. Howald, S. Jha, R.
850 Johnson, P. Kapranov, B. King, C. Kingswood, O. J. Luo, E. Park, K. Persaud, J. B.
851 Preall, P. Ribeca, B. Risk, D. Robyr, M. Sammeth, L. Schaffer, L. H. See, A. Shahab, J.
852 Skancke, A. M. Suzuki, H. Takahashi, H. Tilgner, D. Trout, N. Walters, H. Wang, J.
853 Wrobel, Y. Yu, X. Ruan, Y. Hayashizaki, J. Harrow, M. Gerstein, T. Hubbard, A.
854 Reymond, S. E. Antonarakis, G. Hannon, M. C. Giddings, Y. Ruan, B. Wold, P.
855 Carninci, R. Guigo and T. R. Gingeras (2012). "Landscape of transcription in
856 human cells." *Nature* **489**(7414): 101-108. DOI: 10.1038/nature11233
- 857
- 858 Gallardo, E., A. Navarro, N. Vinolas, R. M. Marrades, T. Diaz, B. Gel, A. Quera, E.
859 Bandres, J. Garcia-Foncillas, J. Ramirez and M. Monzo (2009). "miR-34a as a
860 prognostic marker of relapse in surgically resected non-small-cell lung cancer."
861 *Carcinogenesis* **30**(11): 1903-1909. DOI: 10.1093/carcin/bgp219
- 862

- 863 Hunten, S., M. Kaller, F. Drepper, S. Oeljeklaus, T. Bonfert, F. Erhard, A. Dueck, N.
864 Eichner, C. C. Friedel, G. Meister, R. Zimmer, B. Warscheid and H. Hermeking
865 (2015). "p53-Regulated Networks of Protein, mRNA, miRNA, and lncRNA
866 Expression Revealed by Integrated Pulsed Stable Isotope Labeling With Amino
867 Acids in Cell Culture (pSILAC) and Next Generation Sequencing (NGS) Analyses."
868 Mol Cell Proteomics **14**(10): 2609-2629. DOI: 10.1074/mcp.M115.050237
869
- 870 International Human Genome Sequencing, C. (2004). "Finishing the euchromatic
871 sequence of the human genome." Nature **431**(7011): 931-945. DOI:
872 10.1038/nature03001
873
- 874 Johnsson, P., A. Ackley, L. Vidarsdottir, W. O. Lui, M. Corcoran, D. Grander and K.
875 V. Morris (2013). "A pseudogene long-noncoding-RNA network regulates PTEN
876 transcription and translation in human cells." Nat Struct Mol Biol **20**(4): 440-
877 446. DOI: 10.1038/nsmb.2516
878
- 879 Katayama, S., Y. Tomaru, T. Kasukawa, K. Waki, M. Nakanishi, M. Nakamura, H.
880 Nishida, C. C. Yap, M. Suzuki, J. Kawai, H. Suzuki, P. Carninci, Y. Hayashizaki, C.
881 Wells, M. Frith, T. Ravasi, K. C. Pang, J. Hallinan, J. Mattick, D. A. Hume, L. Lipovich,
882 S. Batalov, P. G. Engstrom, Y. Mizuno, M. A. Faghihi, A. Sandelin, A. M. Chalk, S.
883 Mottagui-Tabar, Z. Liang, B. Lenhard, C. Wahlestedt, R. G. E. R. Group, G. Genome
884 Science and F. Consortium (2005). "Antisense transcription in the mammalian
885 transcriptome." Science **309**(5740): 1564-1566. DOI: 10.1126/science.1112009
886
- 887 Kent, W. J., C. W. Sugnet, T. S. Furey, K. M. Roskin, T. H. Pringle, A. M. Zahler and D.
888 Haussler (2002). "The human genome browser at UCSC." Genome Res **12**(6):
889 996-1006. DOI: 10.1101/gr.229102. Article published online before print in May
890 2002
891
- 892 Kim, K. H., H. J. Kim and T. R. Lee (2017). "Epidermal long non-coding RNAs are
893 regulated by ultraviolet irradiation." Gene **637**: 196-202. DOI:
894 10.1016/j.gene.2017.09.043
895
- 896 Kong, L., Y. Zhang, Z. Q. Ye, X. Q. Liu, S. Q. Zhao, L. Wei and G. Gao (2007). "CPC:
897 assess the protein-coding potential of transcripts using sequence features and
898 support vector machine." Nucleic Acids Res **35**(Web Server issue): W345-349.
899 DOI: 10.1093/nar/gkm391
900
- 901 Lal, A., M. P. Thomas, G. Altschuler, F. Navarro, E. O'Day, X. L. Li, C. Concepcion, Y.
902 C. Han, J. Thiery, D. K. Rajani, A. Deutsch, O. Hofmann, A. Ventura, W. Hide and J.
903 Lieberman (2011). "Capture of microRNA-bound mRNAs identifies the tumor
904 suppressor miR-34a as a regulator of growth factor signaling." PLoS Genet **7**(11):
905 e1002363. DOI: 10.1371/journal.pgen.1002363
906
- 907 Leveille, N., C. A. Melo, K. Rooijers, A. Diaz-Lagares, S. A. Melo, G. Korkmaz, R.
908 Lopes, F. Akbari Moqadam, A. R. Maia, P. J. Wijchers, G. Geeven, M. L. den Boer, R.
909 Kalluri, W. de Laat, M. Esteller and R. Agami (2015). "Genome-wide profiling of
910 p53-regulated enhancer RNAs uncovers a subset of enhancers controlled by a
911 lncRNA." Nature Communications **6**: 6520. DOI: 10.1038/ncomms7520

912
913 Liu, C., K. Kelnar, B. Liu, X. Chen, T. Calhoun-Davis, H. Li, L. Patrawala, H. Yan, C.
914 Jeter, S. Honorio, J. F. Wiggins, A. G. Bader, R. Fagin, D. Brown and D. G. Tang
915 (2011). "The microRNA miR-34a inhibits prostate cancer stem cells and
916 metastasis by directly repressing CD44." *Nat Med* **17**(2): 211-215. DOI:
917 10.1038/nm.2284
918
919 Memczak, S., M. Jens, A. Elefsinioti, F. Torti, J. Krueger, A. Rybak, L. Maier, S. D.
920 Mackowiak, L. H. Gregersen, M. Munschauer, A. Loewer, U. Ziebold, M.
921 Landthaler, C. Kocks, F. le Noble and N. Rajewsky (2013). "Circular RNAs are a
922 large class of animal RNAs with regulatory potency." *Nature* **495**(7441): 333-
923 338. DOI: 10.1038/nature11928
924
925 O'Leary, N. A., M. W. Wright, J. R. Brister, S. Ciufo, D. Haddad, R. McVeigh, B.
926 Rajput, B. Robbertse, B. Smith-White, D. Ako-Adjei, A. Astashyn, A. Badretdin, Y.
927 Bao, O. Blinkova, V. Brover, V. Chetvernin, J. Choi, E. Cox, O. Ermolaeva, C. M.
928 Farrell, T. Goldfarb, T. Gupta, D. Haft, E. Hatcher, W. Hlavina, V. S. Joardar, V. K.
929 Kodali, W. Li, D. Maglott, P. Masterson, K. M. McGarvey, M. R. Murphy, K. O'Neill,
930 S. Pujar, S. H. Rangwala, D. Rausch, L. D. Riddick, C. Schoch, A. Shkeda, S. S. Storz,
931 H. Sun, F. Thibaud-Nissen, I. Tolstoy, R. E. Tully, A. R. Vatsan, C. Wallin, D. Webb,
932 W. Wu, M. J. Landrum, A. Kimchi, T. Tatusova, M. DiCuccio, P. Kitts, T. D. Murphy
933 and K. D. Pruitt (2016). "Reference sequence (RefSeq) database at NCBI: current
934 status, taxonomic expansion, and functional annotation." *Nucleic Acids Res*
935 **44**(D1): D733-745. DOI: 10.1093/nar/gkv1189
936
937 Ozsolak, F., P. Kapranov, S. Foissac, S. W. Kim, E. Fishilevich, A. P. Monaghan, B.
938 John and P. M. Milos (2010). "Comprehensive polyadenylation site maps in yeast
939 and human reveal pervasive alternative polyadenylation." *Cell* **143**(6): 1018-
940 1029. DOI: 10.1016/j.cell.2010.11.020
941
942 Polson, A., E. Durrett and D. Reisman (2011). "A bidirectional promoter reporter
943 vector for the analysis of the p53/WDR79 dual regulatory element." *Plasmid*
944 **66**(3): 169-179. DOI: 10.1016/j.plasmid.2011.08.004
945
946 Rashi-Elkeles, S., H. J. Warnatz, R. Elkon, A. Kupershtein, Y. Chobod, A. Paz, V.
947 Amstislavskiy, M. Sultan, H. Safer, W. Nietfeld, H. Lehrach, R. Shamir, M. L. Yaspo
948 and Y. Shiloh (2014). "Parallel profiling of the transcriptome, cistrome, and
949 epigenome in the cellular response to ionizing radiation." *Sci Signal* **7**(325): rs3.
950 DOI: 10.1126/scisignal.2005032
951
952 Raver-Shapira, N., E. Marciano, E. Meiri, Y. Spector, N. Rosenfeld, N. Moskovits, Z.
953 Bentwich and M. Oren (2007). "Transcriptional activation of miR-34a
954 contributes to p53-mediated apoptosis." *Mol Cell* **26**(5): 731-743. DOI:
955 10.1016/j.molcel.2007.05.017
956
957 Rinn, J. L., M. Kertesz, J. K. Wang, S. L. Squazzo, X. Xu, S. A. Brugmann, L. H.
958 Goodnough, J. A. Helms, P. J. Farnham, E. Segal and H. Y. Chang (2007).
959 "Functional demarcation of active and silent chromatin domains in human HOX

960 loci by noncoding RNAs." *Cell* **129**(7): 1311-1323. DOI:
961 10.1016/j.cell.2007.05.022
962
963 Rokavec, M., M. G. Oner, H. Li, R. Jackstadt, L. Jiang, D. Lodygin, M. Kaller, D. Horst,
964 P. K. Ziegler, S. Schwitalla, J. Slotta-Huspenina, F. G. Bader, F. R. Greten and H.
965 Hermeking (2015). "Corrigendum. IL-6R/STAT3/miR-34a feedback loop
966 promotes EMT-mediated colorectal cancer invasion and metastasis." *J Clin Invest*
967 **125**(3): 1362. DOI: 10.1172/JCI81340
968
969 Schneider, C. A., W. S. Rasband and K. W. Eliceiri (2012). "NIH Image to ImageJ:
970 25 years of image analysis." *Nat Methods* **9**(7): 671-675.
971
972 Serviss, J. T. (2017). miR34AasRNaproject.
973 https://github.com/GranderLab/miR34a_asRNA_project
974
975 Serviss, J. T., P. Johnsson and D. Grander (2014). "An emerging role for long non-
976 coding RNAs in cancer metastasis." *Front Genet* **5**: 234. DOI:
977 10.3389/fgene.2014.00234
978
979 Slabakova, E., Z. Culig, J. Remsik and K. Soucek (2017). "Alternative mechanisms
980 of miR-34a regulation in cancer." *Cell Death Dis* **8**(10): e3100. DOI:
981 10.1038/cddis.2017.495
982
983 Stahlhut, C. and F. J. Slack (2015). "Combinatorial Action of MicroRNAs let-7 and
984 miR-34 Effectively Synergizes with Erlotinib to Suppress Non-small Cell Lung
985 Cancer Cell Proliferation." *Cell Cycle* **14**(13): 2171-2180. DOI:
986 10.1080/15384101.2014.1003008
987
988 Su, X., D. Chakravarti, M. S. Cho, L. Liu, Y. J. Gi, Y. L. Lin, M. L. Leung, A. El-Naggar,
989 C. J. Creighton, M. B. Suraokar, I. Wistuba and E. R. Flores (2010). "TAp63
990 suppresses metastasis through coordinate regulation of Dicer and miRNAs."
991 *Nature* **467**(7318): 986-990. DOI: 10.1038/nature09459
992
993 Sun, F., H. Fu, Q. Liu, Y. Tie, J. Zhu, R. Xing, Z. Sun and X. Zheng (2008).
994 "Downregulation of CCND1 and CDK6 by miR-34a induces cell cycle arrest."
995 *FEBS Lett* **582**(10): 1564-1568. DOI: 10.1016/j.febslet.2008.03.057
996
997 Team, R. C. (2017). "R: A Language and Environment for Statistical Computing."
998 from <https://www.R-project.org/>.
999
1000 Turner, A. M., A. M. Ackley, M. A. Matrone and K. V. Morris (2012).
1001 "Characterization of an HIV-targeted transcriptional gene-silencing RNA in
1002 primary cells." *Hum Gene Ther* **23**(5): 473-483. DOI: 10.1089/hum.2011.165
1003
1004 Vogt, M., J. Mundig, M. Gruner, S. T. Liffers, B. Verdoodt, J. Hauk, L.
1005 Steinstraesser, A. Tannapfel and H. Hermeking (2011). "Frequent concomitant
1006 inactivation of miR-34a and miR-34b/c by CpG methylation in colorectal,
1007 pancreatic, mammary, ovarian, urothelial, and renal cell carcinomas and soft

1008 tissue sarcomas." *Virchows Arch* **458**(3): 313-322. DOI: 10.1007/s00428-010-
1009 1030-5
1010
1011 Wang, L., P. Bu, Y. Ai, T. Srinivasan, H. J. Chen, K. Xiang, S. M. Lipkin and X. Shen
1012 (2016). "A long non-coding RNA targets microRNA miR-34a to regulate colon
1013 cancer stem cell asymmetric division." *eLife* **5**. DOI: 10.7554/eLife.14620
1014
1015 Wang, L., H. J. Park, S. Dasari, S. Wang, J. P. Kocher and W. Li (2013). "CPAT:
1016 Coding-Potential Assessment Tool using an alignment-free logistic regression
1017 model." *Nucleic Acids Res* **41**(6): e74. DOI: 10.1093/nar/gkt006
1018
1019 Wang, X., J. Li, K. Dong, F. Lin, M. Long, Y. Ouyang, J. Wei, X. Chen, Y. Weng, T. He
1020 and H. Zhang (2015). "Tumor suppressor miR-34a targets PD-L1 and functions
1021 as a potential immunotherapeutic target in acute myeloid leukemia." *Cell Signal*
1022 **27**(3): 443-452. DOI: 10.1016/j.cellsig.2014.12.003
1023
1024 Wickham, H. (2016). gtable: Arrange 'Grobs' in Tables. R package version 0.2.0.
1025 <https://CRAN.R-project.org/package=gtable>
1026
1027 Wickham, H. (2017). scales: Scale Functions for Visualization. R package version
1028 0.5.0. <https://CRAN.R-project.org/package=scales>
1029
1030 Wickham, H. (2017). tidyverse: Easily Install and Load the 'Tidyverse'. R package
1031 version 1.2.1. <https://CRAN.R-project.org/package=tidyverse>
1032
1033 Wickham, L. H. a. H. (2017). rlang: Functions for Base Types and Core R and
1034 'Tidyverse' Features. R package version 0.1.4. [https://CRAN.R-
1035 project.org/package=rlang](https://CRAN.R-project.org/package=rlang)
1036
1037 Wickham, S. M. B. a. H. (2014). magrittr: A Forward-Pipe Operator for R. R
1038 package version 1.5. <https://CRAN.R-project.org/package=magrittr>
1039
1040 Wilkins, D. ggenes: Draw Gene Arrow Maps in 'ggplot2'. R package version
1041 0.2.0.9003. <https://github.com/wilkox/ggenes>
1042
1043 Xiao, N. (2017). liftr: Containerize R Markdown Documents. R package version
1044 0.7. <https://CRAN.R-project.org/package=liftr>
1045
1046 Xie, Y. (2017). knitr: A General-Purpose Package for Dynamic Report Generation
1047 in R. R package version 1.17. <https://yihui.name/knitr/>
1048
1049 Yang, P., Q. J. Li, Y. Feng, Y. Zhang, G. J. Markowitz, S. Ning, Y. Deng, J. Zhao, S.
1050 Jiang, Y. Yuan, H. Y. Wang, S. Q. Cheng, D. Xie and X. F. Wang (2012). "TGF-beta-
1051 miR-34a-CCL22 signaling-induced Treg cell recruitment promotes venous
1052 metastases of HBV-positive hepatocellular carcinoma." *Cancer Cell* **22**(3): 291-
1053 303. DOI: 10.1016/j.ccr.2012.07.023
1054
1055 Yap, K. L., S. Li, A. M. Munoz-Cabello, S. Raguz, L. Zeng, S. Mujtaba, J. Gil, M. J.
1056 Walsh and M. M. Zhou (2010). "Molecular interplay of the noncoding RNA ANRIL

1057 and methylated histone H3 lysine 27 by polycomb CBX7 in transcriptional
1058 silencing of INK4a." Mol Cell **38**(5): 662-674. DOI: 10.1016/j.molcel.2010.03.021
1059
1060 Yu, W., D. Gius, P. Onyango, K. Muldoon-Jacobs, J. Karp, A. P. Feinberg and H. Cui
1061 (2008). "Epigenetic silencing of tumour suppressor gene p15 by its antisense
1062 RNA." Nature **451**(7175): 202-206. DOI: 10.1038/nature06468
1063
1064 Zenz, T., J. Mohr, E. Eldering, A. P. Kater, A. Buhler, D. Kienle, D. Winkler, J. Durig,
1065 M. H. van Oers, D. Mertens, H. Dohner and S. Stilgenbauer (2009). "miR-34a as
1066 part of the resistance network in chronic lymphocytic leukemia." Blood **113**(16):
1067 3801-3808. DOI: 10.1182/blood-2008-08-172254
1068
1069